SYNTHESIS OF INORGANIC NANOSCALE CLUSTERS AND HOW THEIR FUNDAMENTAL COORDINATION GEOMETRIES AFFECT SOLUTION SPECIATION AND THIN FILM PROPERTIES

by

BRANTLY LAMAR FULTON

A DISSERTATION

Presented to the Department of Chemistry and Biochemistry
and the Graduate School of the University of Oregon
in Partial Fulfillment of the Requirements
for the degree of
Doctor of Philosophy

June 2019

DISSERTATION APPROVAL PAGE

Student: Brantly Lamar Fulton

Title: Synthesis of Aqueous Inorganic Nanoscale Clusters and how their Coordination Geometries Affect Solution Speciation and Thin Film Properties

This dissertation has been accepted and approved in partial fulfillment of the requirements for the Doctor of Philosophy degree in the Department of Chemistry and Biochemistry by:

Shannon W. Boettcher	Chairperson
James E. Hutchison	Advisor
Darren W. Johnson	Advisor
Victoria J. DeRose	Core Member
James M. Watkins	Institutional Representative

and

Janet Woodruff-Borden	Vice Provost and Dean of the Graduate School

Original approval signatures are on file with the University of Oregon Graduate School.

Degree awarded June 2019

DISSERTATION ABSTRACT

Brantly Lamar Fulton

Doctor of Philosophy

Department of Chemistry and Biochemistry

June 2019

Title: Synthesis of Aqueous Inorganic Nanoscale Clusters and how their Coordination Geometries Affect Solution Speciation and Thin Film Properties

The objective of this thesis research is to understand how fundamental coordination geometry of aqueous nanoscale inorganic clusters effects solution speciation. While past research has developed a substantial understanding of inorganic nanoscale clusters in the solid state less is understood about their dynamic solution phase behavior. This research is designed to make a deliberate approach toward a better understanding of aluminum, scandium, and gallium cluster formation through a mineral dissolution approach while using both solution and solid-state characterization techniques.

Many of these unique clusters formed by this process serve as solution precursors for solution processed metal oxide thin films. Taking advantage of a facile, high yield, scalable mineral dissolution process will allow for robust characterization of metal oxide thin films in the solid state. The mineral dissolution approach applied herein offers new insight into how coordination geometry of clusters in the solution state is not only affected by concentration and pH but also how manipulation of these cluster types determines the electronic properties of their resultant metal oxide thin films by an aqueous solution process.

The outcomes of this research will help bridge the gap between the inorganic chemistry and geochemistry communities by keenly identifying species that are pertinent to both subfields. Additionally, the usage of these clusters as solution precursors for device fabrication will help merge the inorganic solution and solid-state communities. While the mineral dissolution approach applied here will mostly relate to aluminum and scandium cluster systems it can more broadly be applied across the periodic table and will serve as a platform for better understanding of more complex metal systems while still allowing for

the fabrication of aqueous based metal oxide materials towards the design of applications that will affect both our modern and future world. This dissertation includes previously published (unpublished) co-authored material.

CURRICULUM VITAE

NAME OF AUTHOR: Brantly Lamar Fulton

GRADUATE AND UNDERGRADUATE SCHOOLS ATTENDED:

University of Oregon, Eugene, Oregon
Morehouse College, Atlanta, Georgia

DEGREES AWARDED:

Doctor of Philosophy, Chemistry, 2019, University of Oregon
Bachelor of Science, Chemistry, 2013, Morehouse College

AREAS OF SPECIAL INTEREST:

Green materials chemistry
Nanoscale cluster chemistry
Inorganic chemistry
Polynuclear NMR
Metal oxide thin films

PROFESSIONAL EXPERIENCE:

Co-Founder, LAMAR Enterprises LLC, 2018-present
Research Chemist Intern, Cabot Microelectronics, 2017
Graduate Research Fellow, University of Oregon, 2013-2019
Undergraduate Research Fellow, Georgia Institute of Technology, 2009-2013

GRANTS, AWARDS, AND HONORS:

Phil and Penny Knight Campus Research Fellow, University of Oregon, 2017-present
Center for Sustainable Materials Chemistry (CSMC) Research Fellow, University of Oregon
2013-2019
CSMC Informal Science Education Fellow, University of Oregon, 2014-2018
Lens of the Market Alumnus, University of Oregon, 2016
Oregon Museum of Science and Industry (OMSI) Science Communication Fellow, 2014
Promising Scholar Fellow, University of Oregon, 2013
Summer Research Fellow, SURF, University of California, Irvine, 2012
Summer Research Fellow, SPUR, University of Oregon, 2011
Summer Research Fellow, HBCU-Up, Morehouse College, 2009

PATENTS AND PUBLICATIONS:

Application No. 62/190,676. Full Patent Submitted, Awaiting Assignment. "Synthesis of M_{13} Clusters from Aluminum and Gallium Mineral Polymorphs" Assignees: Brantly L. Fulton, Cory K. Perkins, Milton N. Jackson, Shannon W. Boettcher, James E. Hutchison. Douglas A. Keszler, and Darren W. Johnson. **2016**

Perkins, C. K.; Eitrheim, E. S.; Fulton, B. L.; Fullmer, L. B.; Colla, C. A.; Park, D.-H.; Oliveri, A. F.; Hutchison, J. E.; Nyman, M.; Casey, W. H.; Forbes, T.Z.; Johnson, D.W.; Keszler, D.A. Synthesis of an Aluminum Hydroxide Octamer through a Simple Dissolution Method. *Angew. Chemie Int. Ed.* **2017**, *56* (34), 10161–10164 DOI: 10.1002/anie.201702318.

Fulton, B. L.; Perkins, C. K.; Mansergh, R. H.; Jenkins, M. A.; Gouliouk, V.; Jackson, M. N.; Ramos, J. C.; Rogovoy, N. M.; Gutierrez-Higgins, M. T.; Boettcher, S. W.; Conley, J. F.; Keszler, D. A.; Hutchison, J. E.; Johnson D. W. Minerals to Materials: Bulk Synthesis of Aqueous Aluminum Clusters and Their Use as Precursors for Metal Oxide Thin Films. *Chem. Mater.* **2017**, acs.chemmater.7b02106 DOI: 10.1021/acs.chemmater.7b02106.

Perkins, C. K.; Colla, C. A.; Fulton, B. L.; Pilgrim C. D.; Oliveri, A. F.; Hutchison, J. E.; Johnson, D.W.; Synthesis of Al_{13}-Keggin Ions by Dissolution of Aluminum Hydroxide **In Prep, 2018.**

Fulton, B.L.; Cochran, E. A.; Perkins, C. K.; Rogovoy, N. M.; Cheong, P.H.; Boettcher, S. W.; Keszler, D. A.; Hutchison, J. E.; Johnson D. W. Casey, W. H.; Synthesis and Characterization of $[Sc_2(\mu\text{-}OH)_2(H_20)_6(NO_3)_2](NO_3)_2$ by Dissolution and its use as a Precursor for Sc_2O_3 Thin Films **In Prep**, **2019.**

ACKNOWLEDGMENTS

It is too difficult to thank all the people who have helped make this possible over the years individually, but this is my attempt to thank some of those people. I remember being a sophomore chemistry major at Morehouse College sitting in my dorm room watching YouTube videos of a chemist, speaking about the future of nanomaterials in our clothes and textiles. I immediately emailed this professor out of curiosity. This was Prof. Jim Hutchison, who ultimately became one of my thesis advisors here at the University of Oregon. He never responded to the email I sent back then but this was a moment that taught me persistence and how to go over the things that I wanted in life. I was able to connect with Dr. Peter O'Day and the SPUR program at the UO and that connection became one of the most valuable in my network, thank you Peter for that. Through Peter I met Prof. Darren Johnson, my other thesis advisor. I will never forget the first conversation we had over the phone, it mostly consisted of chemistry, college football scores, and how delicious Texas BBQ is. Darren I could have not made it this far without your teaching, support, and guidance, both as a research advisor and helping me in my personal life countless times.

To all the wonderful colleagues that I have been able to work with along this journey, I must thank you. Dr. Cory Perkins, I remember when we first met at a Center for Sustainable Materials Chemistry (CSMC) outreach event in Corvallis, OR. We exchanged contact info and the rest has been history. You helped me so much as a research mentor and helping get our first publications out. I cannot thank you enough for your support in professional and personal life, a true friend I have in you. To Dr. Susan Cooper, Brandon Crockett, and Meredith Sharps, thank you for inspiring me to join the Dutch lab. I felt comfortable and confident that I could achieve because your belief in my abilities helped propel me forward. Dr. Jimmy McDermott and Will Storck thank you for being my best friends throughout my graduate career. The memories that we have shared together are enumerable. Thanks for the honesty and purity in your messages and being there for me at some of the times where I needed friendship and tough love the most. To Dr. Justin

McClinton and Theodore Hicks our friendships will never be broken. Michael Cutrer, thank you for the sacrifices to help get our company LAMAR off the ground. Thank you for being my friend through great times and doubling down through bad times.

I would like to thank my mentee, Nichole Rogovoy. Nichole you taught me so much about mentorship and leadership and you helped re-ignite my own excitement about the gift of discovery. Thank you for being patient as a mentee at a time where I had to learn how to be a good mentor. You will go on to do great things and I am proud to have been a part of your successes.

Lastly, to my immediate family. I would like to thank my brother, Brad Fulton, Jr. When we were kids you always pushed me to be self-sufficient, curious about the world around me, and rooted in morals and ethics over everything else. To my cousin Brandon Gallimore, the bond between us is more than brotherly. Thank you for all the contributions and supporting me through the hard journey of becoming a man. Your work ethic is second to none, and your loyalty has proved to be unconditional. To my parents Brad and Ann Fulton, none of this would be possible without your love, honesty, and hope in what I could become. Even though we did not live in the best neighborhood, or had access to all the best resources, you two always gave what you had. The warmth when I see your faces is unmatched and I am honored and proud to be your son and vow to make you two proud as long as I am on this Earth. Your sacrifices will never go unnoticed, I could not say thank you enough.

I dedicate this to the Southside Chiefs, it is here where I learned some of the best and toughest lessons about life.

TABLE OF CONTENTS

LIST OF FIGURES

Figure Page

Figure Page

Figure Page

LIST OF TABLES

Table Page

LIST OF SCHEMES

Scheme Page

CHAPTER I

A HISTORY OF AQUEOUS ALUMINUM OXO-HYDROXO CLUSTERS

1.1. INTRODUCTION

Aluminum, the 27th element, is the third most abundant element and the most abundant metal in the earth's crust. Traditionally, this metal is mined from aluminum mineral reserves through the Bayer process.[1–4] While the study of aluminum chemistry dates back to the beginning of the 20th century, its aqueous solution chemistry is still being investigated due to aqueous aluminum species having applications ranging from household cosmetics, such as toothpaste and deodorant, to electronic device displays including: TVs, smart phones, and tablets.[5–8] Therefore, it is safe to say that understanding aluminum's fundamental coordination chemistry in aqueous solutions will help chemists elucidate new aluminum species and potential new applications for this widely used element. This conversation will focus directly on the aqueous chemistry of aluminum oxo-hydroxo clusters and how they will directly impact our next generation of products and applications.

Aluminum oxo-hydroxo clusters belong to a larger class of polyoxometallates (POMs) which are traditionally categorized as molecular frameworks containing metal-oxygen-metal (M-O-M) bridges with known chemical formulas and discrete crystal structures.[9,10,11–13] The history of aluminum based POMs larger than a dimer begins with the work done in 1962 by Johansson and co-workers when the epsilon Keggin aluminum 13 polyoxo-hydroxo cluster (**K-Al$_{13}$**) was first isolated having the known chemical formula

$AlO_4Al_{12}(OH)_{24}(H_2O)_{12}^{7+}$.[14] This cluster contains 13 aluminum ions that are bridged by oxygen and hydroxides. The inner core is a tetrahedrally coordinated aluminum ion while the remaining 12 aluminum ions are broken down into 4 identical trimer oligomeric units that cage the tetrahedral core (Figure 1.1. of **K-Al$_{13}$**).

ε

Figure 1.1. A polyhedral representation of the epsilon Keggin isomer having the polyoxo-hydroxo cation formula AlO4Al12(OH)24(H2O)127+. A central tetrahedral aluminum ion is bridged to 4 oxides . 4 identical trimer units are edge-shared. The non-coordinating sulfate anions have been omitted from this structure for clarity.

To balance the charge of this large poly-oxo-hydroxo cation there are non-coordinating sulfate (SO_4^{2-}) anions. Currently, **K-Al$_{13}$** has only been isolated in the crystal structure with divalent anions. In instances where monovalent ions (NO_3^-, Cl^-) have been employed they have never resulted in the single crystal isolation of a **K-Al$_{13}$** cluster. It is believed that the valency of the anion helps aid in structure formation as well as crystallization of the various aluminum clusters. The work done by Bradley and co-workers, then later studies by Casey et al., advanced upon the original **K-Al$_{13}$** cluster by showing that the tetrahedral aluminum center could be substituted with other metal ions.[15,16,17] This substitution highlights the complex and dynamic solution speciation of

aqueous aluminum chemistry as the central tetrahedral aluminum ion can be substituted for gallium and germanium.[18,19,20]

In 1998 Seichter and co-workers isolated the Mogel aluminum cluster having the formula $[Al_{13}(\mu_3\text{-}OH)_6(\mu_2\text{-}OH)_{18}(H_2O)_{24}]^{15+}$. This structure represents the first representation of what we identify as the "flat" aluminum 13 oxo-hydroxo cluster (**F-Al$_{13}$**) (Figure 1.2).[21]

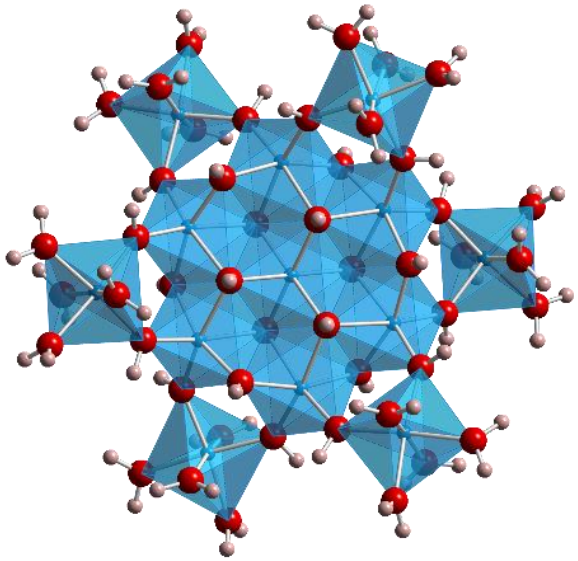

Figure 1.2. A polyhedral representation of the "flat" aluminum 13 cluster having the polyoxo-hydroxo cation formula $[Al_{13}(\mu_3\text{-}OH)_6(\mu_2\text{-}OH)_{18}(H_2O)_{24}]^{15+}$. A central octahedral aluminum ion is bridged to 6 hydroxides. F-Al_{13} has a planar Al_7 core unit and 6 $Al(OH)_2(H_2O)_4$ units that exist above and below the central plane. The non-coordinating chloride anions have been omitted from this structure for clarity.

This work by Seichter and coworkers represents only a couple instances in which this flat aluminum cluster has been isolated in single crystal form with non-coordinating Cl^- anions to balance the charge of the large aluminum polyoxo-cation. **F-Al$_{13}$** is similar to **K-Al$_{13}$** in that it contains exactly 13 aluminum ions but it has a different structural

geometry, charge, and solubility in aqueous environments. In relation to geometry, **F-Al_{13}** has 6 planar aluminum ions that are bridged by hydroxides to the central octahedral aluminum core; there are no tetrahedral sites. The remaining 6 aluminum ions exist above and below the central plane in a rotating fashion. **K-Al_{13}** carries a 7+/8+ charge while **F-Al_{13}** has a 15+ charge, making it the more higher charged species.

The aqueous solubility difference between **K-Al_{13}** and **F-Al_{13}** can be understood by the Baes and Mesmer speciation diagram as well as the Pourbaix diagram for aluminum. The Pourbaix diagram represents potential (eV) versus pH and suggests how aqueous speciation transforms by tuning pH at a constant voltage. Due to aluminum's amphoteric nature, soluble aqueous species exist under acidic and basic conditions, while solid aluminum species ($AlOH_3$) exist between the extremes. Both **K-Al_{13}** and **F-Al_{13}** exist within the acidic regime. **F-Al_{13}** has been observed at lower pH ranges (2.7-3.2) while **K-Al_{13}** species exist at higher pH (3.7-4), this is discussed more in chapters III and IV. Slightly above this pH, aluminum oxo-hydroxo species begin to precipitate out of solution.

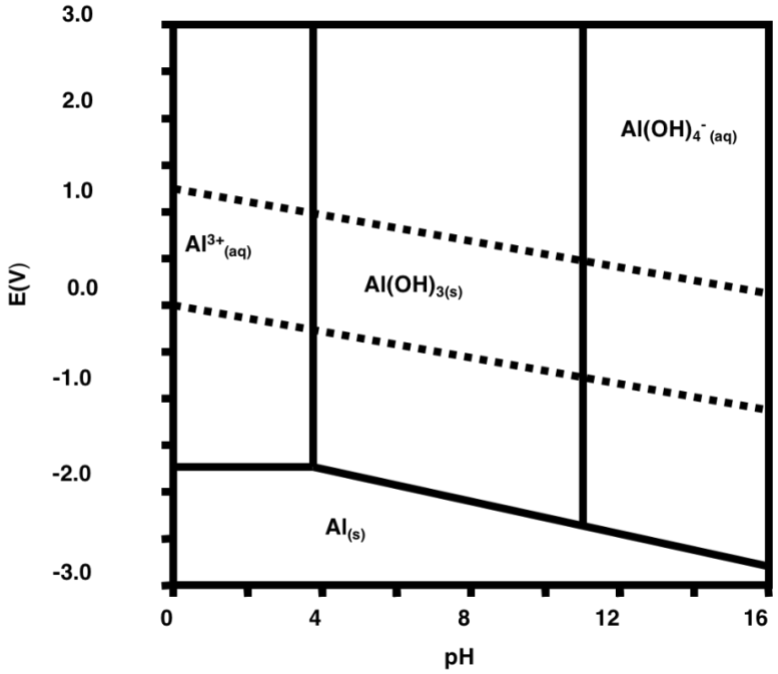

Figure 1.3. The Pourbaix diagram of aluminum.

One of the reasons that **F-Al13** is more acidic than **K-Al13** is due to the fact that aluminum nitrate salts are more acidic and water soluble than aluminum sulfate salts. **K-Al13** is also expected to be the more basic species due to the tetrahedral center, which is similar to the basic tetrahedral ion aluminate ion ($AlOH_4^-$), known to be persistent only under fairly basic conditions (pH = 9-11).

The **F-Al13** work that was done by Seichter and co-workers also provided a foundation for understanding the "flat" gallium 13 oxo-hydroxo cluster's structure (**F-Ga13**) that was first reported by Rather and co-workers in the Darren Johnson group in 2005.[22] **F-Ga13** is iso-structural to the Mogel **F-Al13** polyoxo cation but in isolating the single crystal of this cluster, NO_3^- serves as the charge balancing anion as opposed to Cl^- as in Seichter's work. Briefly, after the isolation of **F-Ga13**, Gatlin and coworkers, also of the Johnson group, were able to isolate the aluminum analog of **F-Ga13** with NO_3^- counter-

anions only when they altered the synthesis to include a small amount of base in the reaction. This represents the first time that **F-Al$_{13}$** had been isolated with NO_3^- counter-anions and set the stage for much of the work that follows within this document.[23]

The work done by Gatlin and co-workers used carcinogenic reagents, namely DBNA as a reductant to slowly increase the pH of aqueous $Al(NO_3)_3$. During slow evaporation, single crystals of the **F-Al$_{13}$** cluster could be isolated in 60% yield. This work was further expanded upon by Wei Wang and co-workers, as they introduced metal Zinc (Zn^0) as the reductant in place of the previously used carcinogens.[24] Using this Zn reduction method they were able to grow and isolate crystals via a slow evaporation method with a 65% yield. While, an increased yield was observed, an additional post-synthesis purification step was also required as $Zn(NO_3)_2$ co-crystalized during this reaction. $Zn(NO_3)_2$ impurities were washed away with isopropanol (IPA).

In another offering Wang and co-workers expounded upon the previous **F-Al$_{13}$** cluster with an electrochemical synthetic method that showed by applying a constant voltage to the aqueous $Al(NO_3)_3$ solution NO_3^- ions could be reduced while the pH of the solution increased until it produced **F-Al$_{13}$** in an electrochemical cell.[25] This offering created the first synthesis in which **F-Al$_{13}$** could be observed without single crystal isolation as compared to the previous work. This electrochemistry route also required no post-synthesis purification methods and potentially set the stage to show how **F-Al$_{13}$** could be used as a precursor for Al_2O_3 thin films.

Kamunde-Devonish, Jackson and co-workers were the first to perform a metallic substitution on the **F-Al$_{13}$** cluster when they isolated the transmetallated aluminum/indium

oxo-hydroxo cluster (**F-Al$_7$In$_6$**).[26] While the central octahedral aluminum core is still hydroxy-bridged to 6 planar aluminum ions, the exterior ring is now substituted with 6 indium ions that exist above and below the central plane. Further tuning the ratio of aluminum to indium did not result in **Al$_X$In$_Y$** clusters where indium was located within the central core, and to this point all-indium oxo-hydroxo clusters have remained elusive. Using a Zn reduction method they were able to combine crystals of the **F-Al$_{13}$** cluster with an aqueous $In(NO_3)_3$ solution undergoing slow evaporation. Single crystals of the **F-Al$_7$In$_6$** cluster could be isolated for single crystal XRD while $Al(NO_3)_3$, $In(NO_3)_3$, and $Zn(NO_3)_2$ co-crystallites were removed from solution with IPA. Due to indium having a larger ionic radius in comparison to aluminum and slower exchange rate in aqueous solutions than aluminum, it is likely that upon crystallization the indium ions outcompete the aluminum ions on the outer ring.

The Tori Forbes group has added a handful of aluminum oxo-hydroxo clusters to the toolbox that are larger oligomers than the Al$_{13}$ clusters described previously here. These clusters include **Al$_{26}$** and **Al$_{30}$**. An interesting feature is that these cluster types contain fragments of the **Al$_{13}$** clusters connected together.[27,28] For instance, **Al$_{26}$** contains two corner shared **K-Al$_{13}$** units. Unlike the **K-Al$_{13}$** cluster the coordinating anions are organic ligands, whereas the **Al$_{13}$** clusters are most notably synthesized with inorganic anions. The synthetic routes to produce these clusters are also very different than the slow evaporation methods that were described herein. **Al$_{26}$** and **Al$_{30}$** are made in Par bomb vessels and the crystals were isolated after this system was removed from pressure.

1.2. CHAPTER II BRIDGE

While there have been more exhaustive studies on **Al_{13}** oxo-hydroxo clusters and larger oligomers that combine **Al_{13}** fragment**s**, less is known about the elusive aluminum octamer **(Al_8).** This species was first isolated by Bill Casey and co-workers in 2005 over the course of a multi-year recrystallization.[29] The following work expands upon the **Al_8** cluster by introducing a dissolution synthesis to produce **Al_8** and the accompanying characterization methods which include ^{27}Al nuclear magnetic resonance imaging (NMR), small-angle X-Ray scattering (SAXS). Similar to **K-Al_{13}**, the **Al_8** polycation is stabilized by non-coordinating sulfate anions SO_4^{2-}.

CHAPTER II

SYNTHESIS OF AN ALUMINUM HYDROXIDE OCTAMER THROUGH A SIMPLE DISSOLUTION METHOD

2.1. INTRODUCTION

My contributions to this work included the original experimental design and synthesis using an aluminum sulfate $Al_2(SO_4)_3$ precursor solution that led to the single crystal isolation of the aluminum octamer, $Al_8(OH)_{14}(H_2O)_{18}(SO)_5$ (**Al_8**). Using the dissolution pathway approach, single crystals of the $Al_8(OH)_{14}(H_2O)_{18}(SO)_5$ (**Al_8**) cluster were isolated for analysis by Eric S. Eitrheim. We also utilized ^{27}Al nuclear magnet resonance (NMR) imaging to determine aqueous speciation changes as a function of concentration and pH. Prof. William Casey and the good folks at UC Davis provided us with instrument time and their NMR and lab facilities to conduct a portion of these experiments. Dr. Cory Perkins aided in this work with key synthetic design and isolation of **Al_8**, led the writing of the manuscript, and key ^{27}Al NMR interpretation. Lauren Fullmer provided useful SWAXS (small and wide angle X-ray scattering) studies that helped us understand the radius of gyration. Chris Colla and Anna Oliveri assisted with ^{27}Al NMR studies that helped identity Al_8 in solution. Deok-Hie Park was the lead on electrospray ionization mass spectrometry (ESI-MS) efforts for this work. The results presented herein are published in the journal *Angewandte Chemie* in 2017.

Aqueous aluminum chemistry displays a rich array of oxo-hydroxo clusters, exemplified by *flat*-Al_{13} $[Al_{13}(OH)_{24}(H_2O)_{24}{}^{15+}]$,[1,2] isomers of the Al_{13}-keggin ion

$[Al_{13}O_4(OH)_{24}(H_2O)_{12}]^{7+}$,[3,4] and larger clusters like the Al_{30} cation $[Al_{30}O_8(OH)_{56}(H_2O)_{26}]^{18+}$.[5,6] Although researchers have explored this chemistry for more than a century, novel species continue to emerge. In 2005,[7] Casey and co-workers reported the octameric aluminum hydroxide cluster $Al_8(OH)_{14}(H_2O)_{18}(SO)_5$ (**Al_8**) as a side product of the aqueous synthesis of the aluminum sulfate dimer $Al_2(OH)_2(H_2O)_8(SO_4)_2$. The octamer was harvested from the reaction solution after nearly 7 years.[7] This long period of time raises questions about whether the cluster may be readily synthesized and whether it even exists in solution. A 2016 report[8] describes the second example of an **Al_8** cluster; in this case, the cluster is isolated from an organic solvent and stabilized with trisilanol capping ligands.

To develop a comprehensive understanding of aqueous aluminum chemistry, we must look into scalable synthesis methods and characterize those simple species that exist under consonant reaction conditions. Nature lends insight to potential synthesis methods. Clusters may form along pathways involving dissolution of aluminum hydroxide solids and clays,[9–11] for example, as products of mineral dissolution in low-pH waters caused by acid-mine drainage or acid rain. Here, we exploit this natural pathway to prepare **Al_8** directly and in high yield via dissolution of solid aluminum hydroxide in sulfuric acid. The crystal-producing solutions also aid speciation studies wherein hydroxo and aqua ligands dominate coordination to Al.

Interest in **Al_8** extends to geochemistry and beyond, as the precise knowledge of cluster structures enables model studies of mineral-surface interactions and chemistries. Clusters help us describe the bonding of adsorbates to soil minerals, and they aid studies of reaction kinetics at the molecular scale, thereby avoiding extraordinarily complex experiments with

minerals suspended in liquids. Also, our understanding of hydroxo-Al cluster chemistry guides and advances solution deposition of functional films[12] and improves the performance of high-resolution inorganic nanopatterning.[13]

2.2. EXPERIMENTAL

2.2.1. General procedures for the synthesis of Al_8 via a dissolution approach pathway. Here, we prepare **Al_8** by a top-down synthesis, i.e., by dissolution of $Al(OH)_3 \bullet 0.7H_2O(s)$ in $H_2SO_4(aq)$. Excess $H_2SO_4(aq)$ effects full dissolution of aluminum hydroxide at an $Al:SO_4^{2-}$ ratio of 1:1 and $[Al_{tot}] = 1$ M. The mixture is stirred and heated at 70 ºC until the hydroxide dissolves completely, typically in 24 h. The solution is passed through a 0.4-µm nylon syringe filter into a 20-mL scintillation vial. Crystals grow by slow evaporation in uncapped vials over a period of one to two weeks.

2.3. RESULTS AND DISCUSSION

We find the **Al_8** crystals to be highly twinned, in line with the previous report.[7] We collected diffraction data to confirm that both the unit-cell parameters and the crystal structure (Figure 2.1.) matched earlier findings. The crystals lose water on removal from the growth solution and convert to an amorphous product. Consequently, partially dehydrated crystals exhibit low solubility in water, which makes the reaction mixtures important for study of the existence and persistence of **Al_8** in solution. Previous studies on **Al_8** do not describe characterization of these aqueous solutions.

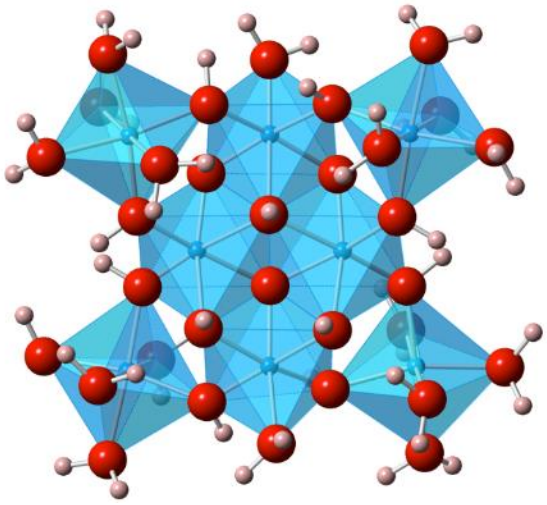

Figure 2.1. Polyhedral structure of the Al_8 cluster (SO_4^{2-} omitted for clarity); blue spheres – Al, red spheres - O, coral spheres – H.

^{27}Al NMR spectroscopy of a 1-M Al reaction solution shows three separate signals (Figure S1). We assign the intense signal centered at 0 ppm to $Al(H_2O)_6^{3+}$ and associated monomeric hydrolysis complexes. The signal at -3.3 ppm corresponds to an inner-sphere sulfato species such as $[Al(H_2O)_5(SO_4)]^+$;[14,15] the spectrum of a 0.5-M $Al_2(SO_4)_3$ solution (Figure S2), for example, also shows this signal. An electrospray ionization mass spectrum (ESI MS, Table S3) of the 1-M Al reaction solution also exhibits signals consistent with a monomeric Al-SO_4^{2-} complex. Its occurrence in the reaction solution likely arises from the excess sulfate added as sulfuric acid, which is required to dissolve solid aluminum hydroxide completely. The third broad signal, centered at +4 ppm, indicates clusters built from six-coordinate aluminum ions. We and others have yet to assign this signal to specific species.[16] One possibility is the cubane-like unit of $Al_3(\mu_3\text{-OH})(\mu_2\text{-OH})_3$, which is found in both **Al_8** and *flat*-Al_{13} clusters.[1,2] **Al_8**, and the structurally similar *flat*-Al_{13}, present aluminum ions bound only by a total of six aqua and hydroxo ligands, i.e., Al does not

directly bind sulfate. In sum, the NMR data suggest the 1-M reaction solution contains a mixture of monomeric and larger hydroxo Al clusters with Al bound exclusively in distorted octahedral environments.

Figure 2.2. shows the ESI-MS data of the 1-M reaction mixture. The spectrum reveals a parent octameric species and several smaller nuclearity species; some of the smaller species likely derive from **Al$_8$** fragmentation during the ionization process. The presence of small clusters, including aluminum-sulfate dimers, is also reasonable, considering the solution

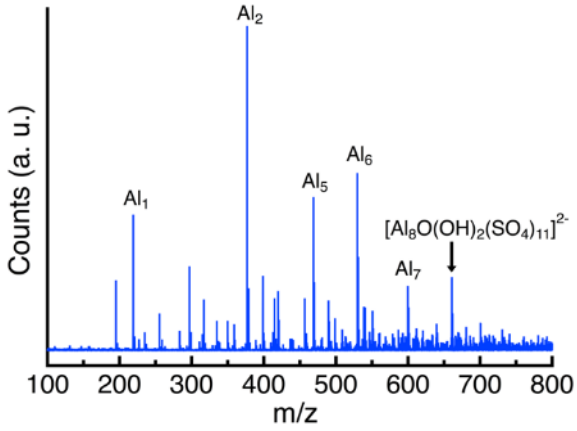

was prepared with excess H_2SO_4 (aq).

Figure 2.2. ESI-MS spectra of the [Al_{tot}] = 1 M solution. Data are normalized to the strongest peak in each spectrum over the selected range. See Table S3 for detailed peak assignments.

To prepare a solution closer to the **Al$_8$** stoichiometry (8:5 ratio of Al:SO_4^{2-}), we increased [Al_{tot}] from 1 to 3 M, following the synthesis procedure described above. The solution pH decreased slightly from 3.37 for the 1-M solution to 3.24 for the 3-M solution. Observationally, the 3-M solution was more viscous, but filtration still produced visually clear solutions for NMR and SWAXS (small and wide angle X-ray scattering) studies.

Figure 3.3. shows the ^{27}Al NMR spectrum of the 3-M solution to be similar to the 1-M solution, although the signals (0 and -3.3 ppm) assigned to monomeric Al are weaker relative to those assigned to the putative clusters (*cf.*, Table S1). Also, the broad signal or set of overlapping signals in the range 4-12 ppm is much broader in the 3-M solution than in the 1-M solution. The broad resonance marks the higher concentration of cluster species built from six-coordinate Al in the concentrated solution. Again, this broad signal suggests **Al$_8$** is likely present in the solution. Overall, the NMR data suggest clusters endure at higher solution concentrations.

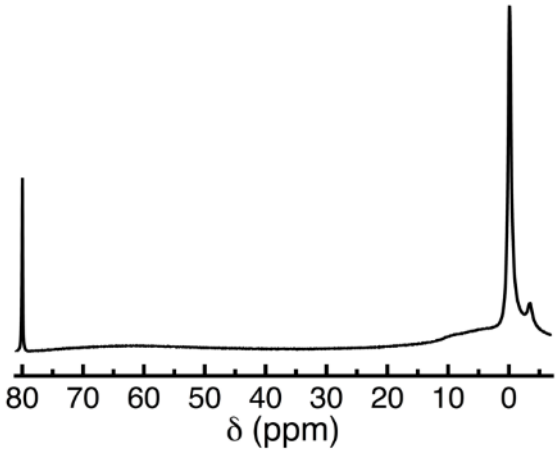

Figure 2.3. ^{27}Al NMR spectrum of 3-M Al solution. The signal at 80 ppm corresponds to the external intensity standard [$Al(OH)_4^-$].

Despite its capabilities for species characterization, X-ray scattering has been applied infrequently to identify clusters in solution.[17–20] It uniquely complements the molecular-scale structural information derived from NMR. Figure S3 shows scattering data for the 1-M Al reaction solution and a simulated curve for **Al$_8$**. The plateau in the experimental curve for q < 0.7 indicates the solution contains nearly monodisperse, spherical species. In the Guinier region (q = 0.06 – 0.5 Å^{-1}), the drop in the solution scattering intensity relative to the simulated curve indicates the presence of scattering species larger than **Al$_8$**.

Figure 2.4. shows SWAXS data for a concentrated 3-M reaction solution. The negative slope in the region q = 0 – 0.2 Å^{-1} indicates a size distribution of species or aggregation arising from the high solution concentration. The Guinier region of the scattering curve (q = 0.2 – 0.6 Å^{-1}) matches the simulated scattering for **Al$_8$** reasonably well. Guinier analysis yields a radius of gyration, a shape independent root mean square of the distance of all electrons from the center of a scattering particle. The derived radius, 6.0 Å, compares to the radius of 6.3 Å for **Al$_8$**. We performed a size-distribution analysis with the scattering data of the 1- and 3-M solutions. Figure S4 and Table S2 show the dominant species in each solution has an average diameter between 10.1 and 10.7 Å, consistent with the long dimension of **Al$_8$.** Secondary species at 14.5-nm diameter in the 1-M solution and 12.8 nm in the 3-M solution reveals the dilute solution has the greater polydispersity, a result anticipated above from the scattering curve (Figure S3).

The 3-M solution readily produces **Al$_8$** crystals in high yield - 84% - which further signals the presence of **Al$_8$** in solution. Bulk elemental analysis shows elemental ratios for **Al$_8$** crystals of Al:S = 8:5.07, close to that of the single-crystal stoichiometry of Al:SO_4 = 8:5. From thermogravimetric analysis, we deduce a stoichiometry of Al:SO_4 = 8:5. In this evaluation, we assume evolution of SO_3(g) dominates mass loss above 425 ºC. ESI-MS on the 3-M solution was considered, but the analysis requires a dilute solution of the cluster. On dilution, however, the solution pH rises, condensation occurs, and a precipitate forms, which obviates the MS analysis. An alternative approach to sample injection must be developed to analyze solutions with the Al:SO_4 = 8:5 ratio of the crystal.

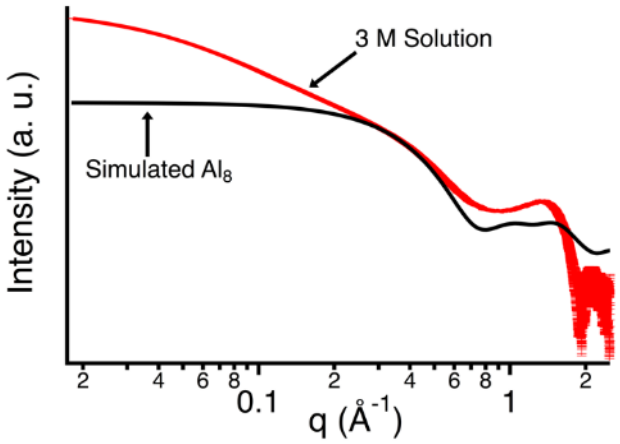

Figure 2.4. SWAXS curve (red) of the 3-M Al solution and simulated curve (black) for **Al$_8$** from the crystal structure file. Data are normalized to the Guinier region to ease comparison.

Because sulfate and selenate are often interchangeable in cluster synthesis,[4,21] we examined synthesis of the SeO_4^{2-} analogue via dissolution of $Al(OH)_3$•$0.7H_2O$(s) in H_2SeO_4(aq). While we were unsuccessful in attempts to crystallize the **Al$_8$** selenate, the ^{27}Al NMR and SWAXS data again suggest clusters exist in the solution (Figures S6-S9). Additional study should reveal the nature of the dominant species in the solutions and whether they mimic those found with sulfate or with weakly coordinating ligands.

We have previously shown the *flat*-Al_{13} cluster serves as a precursor to produce atomically-smooth Al_2O_3 films for both electrical and optical applications.[22,23] **Al$_8$** may be deposited in a similar way to produce an aluminum sulfate film. Electron micrographs (Figure S10) show a featureless, smooth surface with a continuous, pore-free cross section. The film carries morphological features similar to amorphous Al_2O_3.

2.4. CONCLUSIONS

In summary, this study shows the **Al_8** aluminum cluster forms readily by simple dissolution of aluminum hydroxide in sulfuric acid; an observation that mirrors natural processes, namely, the effects of acid rain on soil. The combination of NMR, ESI-MS, and SAXS data reveals **Al_8** persists in both dilute and concentrated solutions. X-ray diffraction results show it readily crystallizes from these solutions in high yield. Together, the solution and crystal-growth findings clarify speciation in an environmentally and technologically important aqueous system, while also confirming the unique structure-directing role of sulfate in aluminum hydroxide cluster chemistry. The study removes potentially confounding effects on speciation from cations introduced via conventional base titrations. The acid-dissolution method enables the first top-down preparation of a simple aluminum hydroxide cluster. The results highlight its efficacy and growing and general applicability.[24–26] Notably, the method supports scale-up needs for high-purity film precursors in materials science.

2.5. CHAPTER III BRIDGE

The aqueous aluminum ocatamer, Al_8 was isolated with sulfate (SO_4^{2-}) anions using a dissolution approach pathway. In the next chapter a similar dissolution approach pathway is used except with nitrate (NO_3^-) anions to produce the aluminum Keggin cluster (**K-Al_{13}**). All 5 **K-Al_{13}** isomers were identified in solution for the first time by ^{27}Al NMR.

CHAPTER III

SYNTHESIS OF A FULL SET OF AL_{13}-KEGGIN ISOMER IONS BY DISSOLUTION OF ALUMINUM HYDROXIDE

3.1. INTRODUCTION

My contributions to this work included the synthetic design process using a dissolution approach pathway that led to the identification of all five aluminum Keggin 13 isomers (**K-Al_{13}**) in a single reaction mixture. We also utilized ^{27}Al nuclear magnet resonance (NMR) imaging to determine speciation of the five **K-Al_{13}** isomers thanks to Prof. William Casey and the good folks at UC Davis provided us with instrument time and their NMR and lab facilities to conduct a portion of these experiments. Dr. Cory Perkins aided in this work with key synthetic design and identification, led the writing of the manuscript, and key ^{27}Al NMR interpretation. Dr. Chris Colla, Dr. Corey Pilgrim, and Dr. Anna Oliveri assisted with ^{27}Al NMR studies that helped identity these species in solution. The results presented herein are unpublished but a manuscript is in preparation for the journal *Angewandte Chemie*.

While aluminum is the second most abundant metal in the Earth's crust, its aqueous hydrolysis chemistry is complicated and poorly understood, in part due to the lack of useful spectroscopic signatures of Al-compounds[1–11]. Aluminum is a hard Lewis acid with a small radius, low-polarizability, and a quadrupolar nucleus that yields broad NMR signals in solution. However, tetrahedrally coordinated aluminums in the center of the Keggin-type aluminum compounds ($Al(O)_4$) are sufficiently symmetric that sharp peaks can be

observed in the ^{27}Al-NMR spectrum. Recently signals were assigned to the various isomers based in part on diffusion rates of the ions and chemical shift values in liquid and solid-state.[12–15]

Chemists typically use aqueous base addition to hydrolyze aluminum cluster compounds, starting from acidic solutions where the $[Al(OH_2)_6]^{3+}$ ion predominates and driving the solution baseward dropwise. We recently demonstrated a method to produce aluminum clusters by dissolving solid $Al(OH)_3$ in mineral acids, thus using the aluminum source, i.e. $Al(OH)_3$, as the base.[16,17] This approach is more gentle than

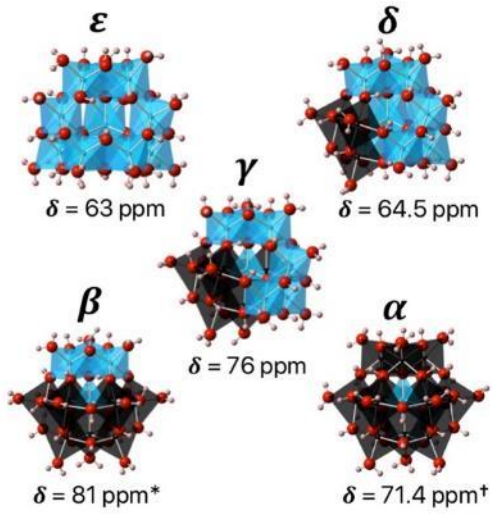

Figure 3.1. Structures of the five isomers of the Keggin-Al_{13}. The black polyhedra are trimeric units that are rotated 60° to a corner-shared geometry from the edge-shared geometry of the ε-isomer. * = hypothesized chemical shift. † = value from ssNMR of the mineral zunyite.

dropwise base addition and allows strict control of the Al:X ratio (X = NO_3^-, Cl^-, SO_4^{2-}, etc.), which results in precise control over speciation. This approach also minimizes pH shock, where disequilibrium transient species form before a drop of high-pH titrant mixes, and also reduces the concentration of background metal species, which could potentially affect properties of the final product. In our previous reports, we demonstrated the synthesis

of the $Al_{13}(\mu_3\text{-}OH)_6(\mu_2\text{-}OH)_{18}(H_2O)_{24}(NO_3)_{15}$ **(*flat*-Al$_{13}$)** and $Al_8(OH)_{14}(H_2O)_{18}(SO_4)_5$ **(Al$_8$)** clusters by dissolution of hydrated $Al(OH)_3$.[16,17] Here we report the synthesis of the series of Keggin-Al_{13} clusters by dissolution of solid $Al(OH)_3 \bullet 0.7H_2O$ and show the ^{27}Al-NMR signals assigned to the five isomers[15] can be recovered even in the absence of alkali and alkaline-earth metals as counterions.

The most commonly studied aluminum cluster is ***ε*-Al$_{13}$** (Fig. 3.1.), due to its ease of synthesis and relative stability.[18] The structure of the ***ε*-Al$_{13}$** consists of four planar trimeric $Al_3(OH)_6$ groups linked to the central $Al(O)_4$ site via four μ_4-O. There are five Keggin isomers that differ only in the number of trimeric units rotated by 60º about the $Al(O)_4$ unit relative to the ***ε*-Al$_{13}$**. With isomerization, bonding between $Al_3(OH)_6$ units change from edge-sharing to corner sharing. Each rotation provides distinct bonding environments of the central $Al(O)_4$ unit, yielding diagnostic chemical shift values for each isomer.

Among the five isomers, the α- and β-isomers have not yet been isolated as a molecule in a simple salt; thus the assignment of these ^{27}Al-signals is based upon indirect evidence. The resonances of the central tetrahedrally coordinated $Al(O)_4$ for these isomers are presumed to be 71.4 and 81 ppm, respectively.[14,19] The **α-Al$_{13}$** cluster (a substructure within the mineral zunyite) has been characterized by solid-state NMR and is the basis for the 71.4 ppm signal for the α-isomer. Recently, we reported the appearance of the 71.4 ppm signal in solutions of ***ε*-Al$_{13}$** and glycine.[15] Researchers have hypothesized the resonance at 81 ppm is due to the **β-Al$_{13}$** isomer, which arises from concomitant changes in chemical shifts by 6 ± 1 ppm with isomerization of Keggin conformers.[20,21] The signal for the ***δ*-Al$_{13}$** is exceptional.

3.2. EXPERIMENTAL

We prepared solutions by dissolving $Al(OH)_3 \bullet 0.7H_2O(s)$ (Alfa Aesar) in 0.54 M $HNO_3(aq)$ (Mallinckrodt) with a 1:0.54 of Al/NO_3^- (or Al/Cl^-). After adding the $Al(OH)_3 \bullet 0.7H_2O$, the slurry was stirred under mild heat (45 ºC) for 72 h to produce a colorless solution. Similarly, we prepared solutions using HCl that gave identical results. High-resolution ^{27}Al NMR experiments were conducted at the UC Davis NMR Facility. Experiments were completed using a Bruker AVANCE DRX-500 NMR spectrometer built around an 11.74 T cryomagnet operating at 130.31 MHz. Data was collected using a DOTY DSI-760 low-aluminum background 10-mm NMR probe

To prepare the Al_{13} Keggin, $Al(OH)_3 \bullet 0.7H_2O(s)$ (4.53 g) was dissolved in 50 mL of 0.54 M HNO_3 (or HCl) to yield a solution where $[Al_{tot}] = 1$ M. This corresponds to a 13:7 Al/NO_3 ratio, consistent with the +7 charge of the ***ε*-Al_{13}**. The reaction was heated at 45 ºC with magnetic stirring. After 72 h, the solution was passed through a 0.2-µm filter. The pH of the solution was 4.1 – consistent with the pH of solutions reported for the ***ε*-Al_{13}** synthesis.[22]

The ^{27}Al NMR spectrum of the as-prepared solution shows the presence of the ***ε*-Al_{13}**, as expected, and characterized by the resonance at 63 ppm (Fig. 2.2.). The broad resonance centered at ~12 ppm can be assigned to the AlO_6 units that surround the tetrahedrally coordinated $Al(O)_4$ center of the Keggin ion. There is always a small signal assignable to $[Al(OH_2)_6]^{3+}$ and octahedral hydrolysis species, with a resonance near 0 ppm. The low intensity resonance centered at 70 ppm is clearly due to the

$Al_{30}O_8(OH)_{56}(H_2O)_{24}^{18+}$ (**Al_{30}**) cation.[5,6] The signal at 80 ppm results from a 40-mM $NaAl(OH)_4$(aq) internal chemical-shift standard.

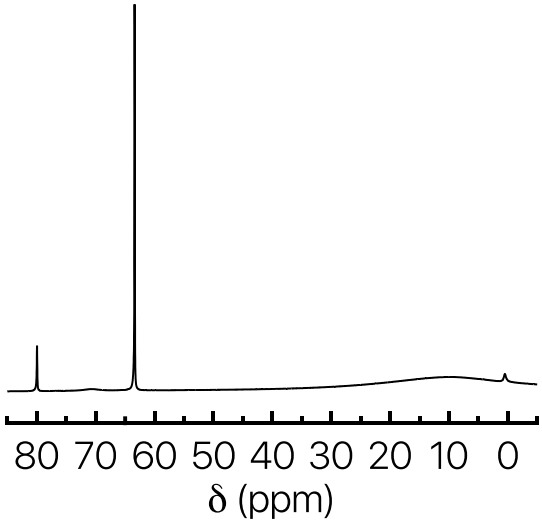

Figure 3.2. ^{27}Al NMR spectrum of the as-prepared solution of Al_{13}-Keggin ion isomers. The signal at 80 ppm is from a 40-mM $NaAl(OH)_4$(aq) internal chemical-shift standard.

To understand how the reaction proceeds, we monitored the dissolution process *in situ* by ^{27}Al NMR (Fig. S1). We show a high concentration of aluminum monomer ions, dominated by $[Al(OH_2)_6]^{3+}$,upon addition of HNO_3(aq) (i.e. signal at 0 ppm). Hydrolysis products form shortly after mixing, indicated by the ~ 4 ppm signal that steadily increases in intensity with time. Thus, ^{27}Al-NMR signals are identical to those found by forced hydrolysis of $[Al(OH_2)_6]^{3+}$ using NaOH titration, although we now produce a solution with aluminum hydrolysis complexes and NO_3 without other countercations.

3.3. RESULTS AND DISCUSSION

Expanding the spectral window around the tetrahedrally coordinated Al region (~55-85 ppm), we observe several ^{27}Al NMR signals (Fig. 3.3.). Beside the high intensity

63 ppm resonance for $\boldsymbol{\varepsilon}$-**Al$_{13}$**, we observe signature resonances assignable to the $\boldsymbol{\delta}$-**Al$_{13}$** (64.5 ppm) and $\boldsymbol{\gamma}$-**Al$_{13}$** (76 ppm).[12,13,21] We also show a very small signal at 81 ppm, that is hypothesized to belong to the **β-Al$_{13}$** isomer.[20] Lastly, we observe a sharp signal on the shoulder of the larger signal that is assigned to the **Al$_{30}$** cation, which is a derivative constructed of two $\boldsymbol{\delta}$-**Al$_{13}$** clusters linked by four bridging AlO_6 units. Following Oliveri et al. we assign this very narrow signal on the shoulder to the **α-Al$_{13}$**, based on the ssNMR signal of the **α-Al$_{13}$** in the mineral zunyite[19] and the size of the diffusing ion that corresponds to this signal (see Oliveri et al.).[15] We have yet to crystallize any of the minor isomer ions from solution and to do so may prove impossible given their identical sizes and charges.

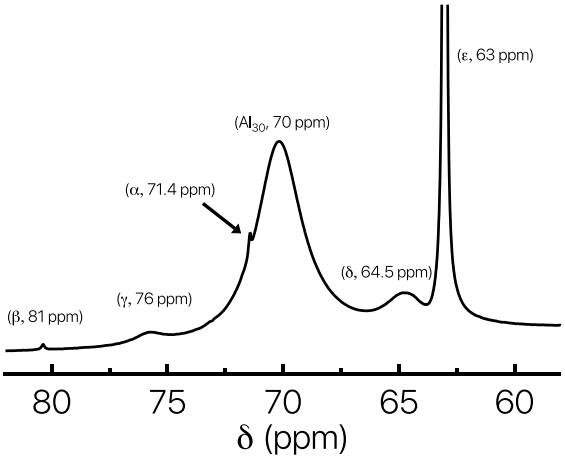

Figure 3.3. Region of interest of the ^{27}Al NMR spectrum for the as-prepared solution featuring resonances for the tetrahedrally coordinated Al ions in each Keggin isomer.

Evidence to date indicates that the ^{27}Al-NMR signal of the $Al(O)_4$ in the isomers is unaffected by atoms on the periphery of the outer $Al_3(OH)_6$ units. Table 1 lists ssNMR chemical shifts of Keggin Al_{13} clusters with various counterions. Chemical shift values of the $Al(O)_4$ site in both $\boldsymbol{\varepsilon}$- and $\boldsymbol{\delta}$-**Al$_{13}$** isomers are unaffected when cocrystallized with

transition metals (including tungsten), and various inorganic, and organic counterions. Correspondingly, we expect that the ^{27}Al-NMR signal for the $Al(O)_4$ site in the mineral zunyite to be a good guide for the **α-Al_{13}** ion. In this mineral the SiO_2 units are removed from the center $Al(O)_4$ unit by four atoms.

Molecule	δ (ppm)	Ref.
[δ-Al_{13}][$H_2W_{12}O_{40}$](OH)•nH_2O	64.7	[23]
[δ-Al_{13}][$CoW_{12}O_{40}$](OH)•nH_2O	64.7	[23]
Na[δ-Al_{13}][2,6NDS$_4$]•13.5H_2O	64.9	[13,24]
Na[δ-Al_{13}][SO_4]$_4$•19H_2O	64.5	[5,6]
[ε-Al_{13}][α-$CoW_{12}O_{40}$]•34H_2O	63	[25]
[ε-Al_{13}][α-1,2,3-$SiV_3W_9O_{40}$]	63	[25]
[ε-Al_{13}][α-1,2,3-H $SiV_3W_9O_{40}$]	63	[25]
[ε-Al_{13}(OC_2H_4OH)$_{12}$]Cl_7·H2O	62.5	[26]
Na[ε-Al_{13}][SO_4]$_4$•12H_2O	63	[14]

Table 3.1. ^{27}Al ssNMR chemical shifts of Al_{13}-Keggin isomers crystalized as different salts, referenced to $Al(NO_3)_3$(aq).

If one accepts the peak assignments, then this report is the first demonstration that isomers of the Al_{13} Keggin ions can form in the absence of alkali and alkaline-earth metals, which were thought to stabilize trimeric unit rotations (e.g., **δ-Al_{13}**).[3,5] This idea arose due to the strong interaction between Na^+ and the η-H_2O of the rotated trimeric unit in the **δ-Al_{13}** structure, and the common cocrystallization of this isomer with a sodium cap. Allouche and Taulelle suggest that isomerization within the series of five isomers is mediated by monomeric $Al(H_2O)_6^{3+}$, interacting in a similar fashion as Na^+.[20] They assign the resonance at 64.5 ppm to an Al-capped multimer ions, though it has been demonstrated elsewhere that the signal belongs to **δ-Al_{13}**.[19] We rule out exchange of Al-monomers with the **Al_{30}** and **Al_{13}**-isomers by the lack of correlation of signals in ^{27}Al EXSY experiments

(Fig. S2). Thus, coordination-assisted-isomerization on the NMR time scale is unlikely in this case.

3.4. CONCLUSION

The result is important because the presence of all five Al_{13} Keggin isomers in the same solution suggests a lower energetic barrier to isomerization than computations suggest.[27]

In this contribution we detail a simple method to produce molecules that we speculate are assignable to the five isomers of the Al_{13} Keggin ions. It is possible that at high Al-concentrations solutions employed in this study are made possible by the absence of coordinating counterions, since similar concentrations in a forced titration would yield amorphous solids. Our method yields a high purity material free of transient species that can be used to generate precursors for catalysis formation and thin-film materials. As synthetic methods and yields improve, we expect to produce structures for X-ray confirmation and thermochemical analysis to understand the relative energies of each of the Al_{13} isomers.

3.5. CHAPTER IV BRIDGE

^{27}Al NMR was a useful tool in helping us identify each of the 5 **K-Al$_{13}$** isomers in a single reaction mixture. This next chapter uses a similar dissolution pathway to observe the persistence of **F-Al$_{13}$** in solution by ^{27}Al NMR under a stoichiometric conditions for **F-Al$_{13}$**. Expanding upon the previous solution studies that have been presented we were able to use a solution based thin film deposition process to characterize Al_2O_3 thin films.

CHAPTER IV

MINERALS TO MATERIALS: BULK SYNTHESIS OF AQUEOUS ALUMINUM CLUSTERS AND THEIR USE AS PRECURSORS FOR METAL OXIDE THIN FILMS

4.1. INTRODUCTION

My contributions to this work included the original experimental design and synthesis as well as characterization techniques to observe the $Al_{13}(\mu_3\text{-}OH)_6(\mu_2\text{-}OH)_{18}(H_2O)_{24}(NO_3)_{15}$ (***flat*-Al$_{13}$**) cluster in the solution state. I also performed solid state Raman spectroscopy to analyze this species. Dr. Cory Perkins who was also a co-author on this work assisted with additional synthetic contributions and solution ^{27}Al NMR. This work could not have been completed without the XRD, TEM, and ellipsometry assistance from Dr. Ryan Mansergh, Melanie Jenkins, Vasiliy Goulioukand Dr. Juan Ramos. Additional sample preparation was provided with the help of Dr. Milton Jackson and Nichole Rogovoy. The results presented herein are published in the journal Chemistry of Materials in 2017.

Aqueous aluminum chemistry is widely studied because of its relevance to many fields of science. As the most abundant metal in the Earth's crust, Al dominates many soils and influences ecotoxicity;[1] hence, its dissolution from clay, rocks, and minerals is fundamentally important. By understanding how to control dissolution of simple Al minerals in the lab, we may gain insight on related processes in nature. Strict control of

solution species and particles may enable new approaches to large-volume, industrially relevant processes like chemical mechanical planarization and catalysis.[2,3]

In their quest to understand aqueous aluminum chemistry, chemists and geochemists have discovered several aluminum hydroxide cluster compounds.[4–11] Among these compounds, the tridecameric cluster, $Al_{13}(\mu_3\text{-}OH)_6(\mu_2\text{-}OH)_{18}(H_2O)_{24}(NO_3)_{15}$ (***flat*-Al_{13}**), has received attention as a precursor for deposition of Al_2O_3 thin films.[12–14] Clusters aid deposition of continuous, smooth, and dense in part because of the preformed metal-oxygen connectivity that facilitates densification.[15–21] Hence, the *flat*-Al_{13} cluster is an attractive precursor to produce dense, aluminum oxide thin films from aqueous solutions.

Typically, aluminum hydroxide clusters are prepared via bottom-up approaches by addition of strong base to acidic solutions of monomeric Al salts; such approaches commonly produce the Keggin-Al_{13} tridecamer. Previous reported approaches to produce ***flat*-Al_{13}** require post-synthesis purification,[9,10] may be difficult to scale to large volumes or both.[22] Here, we report a top-down method to produce the ***flat*-Al_{13}** cluster in high yields (>90%) in >100-g quantities. By directly dissolving high purity $Al(OH)_3$ (gibbsite) in HNO_3(aq) with a ratio of 13:15 Al:NO_3, we address the shortcomings of other methods and eliminate the need for additional purification. We show that the use of this as-prepared solution as a precursor yields high quality, smooth, and amorphous thin films. This approach is a notable improvement over previously reported methods that required the removal of unwanted impurities from reaction mixtures, and suggests the synthetic method could facilitate precursor scale-up for large-area substrate coatings applied to windows, displays, and photovoltaic devices.

4.2. EXPERIMENTAL

$Al(OH)_3 \bullet 0.7H_2O$ gel (Alfa-Aesar) and HNO_3(aq) (Macron Fine Chemicals) were used without further modification. We specifically targeted ***flat*-Al_{13},** which has an Al:NO_3 = 13:15. To prepare a 100-mL solution with a [Al_{tot}] of 1.0 M, we dissolved 9.06 g of $Al(OH)_3 \bullet 0.7H_2O$ in 23.1 mL of 5.0 M HNO_3(aq). After mixing, the solution was stirred at 40 ºC for 24 h, resulting in a clear solution. The solution was filtered through a 0.2-μm membrane to remove residual solids.

The resultant solution was characterized with ^{27}Al NMR, collected on a Bruker 400 MHz DPX-400 spectrometer. Dynamic light scattering (DLS) and phase analysis light scattering (PALS) was used to measure the hydrodynamic radius (R_h). DLS and PALS data were collected on a Möbiuζ Mobility Instrument from Wyatt Technologies. DLS data were collected at room temperature with 532-nm laser light, after passing the solution through a 0.1-μm PTFE filter to ensure removal of residual particles.

The resultant colorless solutions were drop cast on a glass slide and allowed to evaporate at 40 ºC in open air to characterize bulk solid from the precursor. Small crystallites were apparent from an optical microscope. We collected powder X-ray diffraction data on the solid sample, using a Rigaku Ultima IV multipurpose X-ray diffraction system, with Cu Kα radiation. Raman data was collected on the solid sample using an Alpha 300S SNOM confocal Raman microscope in a 180° backscattering configuration. An excitation wavelength of 532 nm was used with a resolution of 1 cm^{-1}. The spectra from each sample were averaged over 100 accumulations at 1 s exposure times. The Raman spectra were referenced to the 520.5 cm^{-1} peak of Si.

Prior to thin-film deposition, all substrates were cleaned by sonication in a deionized water bath. Following this cleaning, they were treated in a low-energy O_2 plasma

for 5 min to create a clean, hydrophilic surface. The films were deposited onto degenerately doped *p*-type Si. Films were deposited by spin coating the aqueous precursors at 3000 rpm for 30 s. Each coat was cured at 230 °C for 1 min before deposition of additional layers. All films were annealed for 1 h at the target temperatures prior to analysis.

Spectroscopic ellipsometry measurements were collected on a J. A. Woollam M-2000 instrument to determine the film thicknesses, which were modeled using the CompleteEASE software package.[32] The Cauchy model was employed to determine the thicknesses and optical constants of the soft baked and annealed thin films. XRD spectra were collected on a Rigaku Ultima IV multipurpose X-ray diffraction system, with Cu Kα radiation. AFM measurements were carried out using an Asylum Research MFP-3D atomic force microscope and images were acquired over 10 × 10 μm^2 areas. FTIR data was collected on a Thermo Fischer Scientific Nicolet 6700 FTIR equipped with diamond ATR.

To emphasize the high-quality nature of the produced thin films, we collected TEM images of a 247-nm thick film, created by depositing five successive coats of the 1-M Al_{tot} solution, baked at 230 ºC between each deposition, and annealed at 500 ºC for 1 h. TEM micrographs were collected on an FEI Titan 80-200 TEM/STEM transmission electron microscope operating at 200 kV. Carbon and chromium coatings were deposited on the a-Al_2O_3 film annealed at 500 ºC for protection during the ion milling process and to enhance sample contrast. After adding a final protective layer of platinum *in situ*, a thin cross section of the film was milled out using the focused gallium ion beam on an FEI Quanta 3D dual beam FIB/SEM. The lamella was welded to a copper TEM grid and then thinned to less than 100 nm and polished at 5 kV using the ion beam.

4.3. RESULTS AND DISCUSSION

We aimed to synthesize ***flat*-Al_{13}** by a direct mineral dissolution process. The stoichiometry of the ***flat*-Al_{13}** observed in its crystal structure guides the synthetic method, as it sets the Al:NO_3 ratio of 13:15, which is readily realized by dissolving $Al(OH)_3$•$0.7H_2O$ in 5 M HNO_3(aq). After dissolution, the pH of the solution is 3.18, falling in the pH range previously reported for the formation of the ***flat*-Al_{13}**.[22] The presence of near-nanometer size particles in solution commonly indicates cluster formation.[23] DLS measurements on the solution shows clusters with an average hydrodynamic radius = 0.8 ± 0.1 nm, a result consistent with previous reports that assign ***flat*-M_{13}** clusters have hydrodynamic radii ranging from 0.9 to 1.0 nm.[14] A broad peak centered at 4 ppm in the solution ^{27}Al NMR spectrum (Figure 4.1.) identifies an oligomeric species containing six-coordinate aluminum, which is also consistent with a previously reported spectrum of ***flat*-Al_{13}**. Importantly, there is only a small downfield peak at 63 ppm, consistent with the ε-Al_{13} Keggin ion, representing a < 2% impurity.[22]

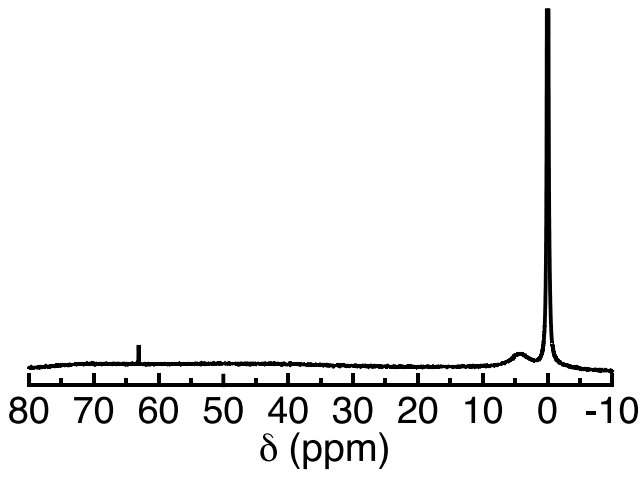

Figure 4.1. ^{27}Al NMR spectrum of the ***flat*-Al_{13}** prepared by dissolution of $Al(OH)_3$

Characterization of the bulk solid isolated from the solution to corroborates that ***flat*-Al$_{13}$** is the dominant species in solution. The cluster containing solution was drop cast on a glass slide and dried at 40 ºC. Figure 2a shows X-ray diffraction data obtained from the resulting solid material closely matches the pattern from bulk ***flat*-Al$_{13}$** described in our previous report.[9] In addition, the inset of Figure 4.2a. reveals crystallites of ***flat*-Al$_{13}$** are easily observed in a confocal microscope image. Raman spectra of these crystallites contains stretches characteristic of ***flat*-Al$_{13}$** (Figure 4.2b.). The Raman bands at 517, 574, and 626 cm^{-1} correspond to Al-(OH)-Al vibrational modes and the symmetric stretch of the ***flat*-Al$_{13}$** cluster appears at 478 cm^{-1}, consistent with the Raman spectra we previously reported for the ***flat*-Al$_{13}$** cluster.[23] We assign the high intensity peak at 1048 cm^{-1} to the symmetric NO_3^- stretch.

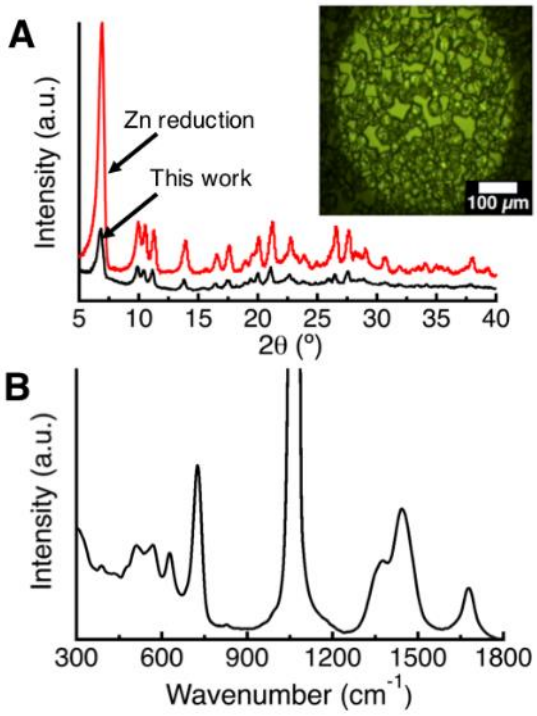

Figure 4.2. (a) Diffraction patterns of polycrystalline ***flat*-Al$_{13}$** from dissolution (black) and the ***flat*-Al$_{13}$** from zinc reduction (red). (b) The Raman spectrum showing characteristic stretches for ***flat*-Al$_{13}$** from dissolution and a confocal microscope image of the crystallites (inset).

The top-down approach allows ready investigation of other monoprotic acids for the dissolution of $Al(OH)_3$ to produce ***flat*-Al_{13}**, which cannot be done with other synthetic routes. For example, Scheme 1 shows reduction of nitrate counterions aids syntheses via electrolysis, Zn reduction, and organic nitroso-containing compounds; thus, synthesis of the ***flat*-Al_{13}** from other reagents such as $AlCl_3$ is energetically unfavorable using the aforementioned methods. The first report of ***flat*-Al_{13}** employed the chloride salt, but the method suffers from a four-and-a-half-month preparation. With the top-down method, we readily synthesize ***flat*-Al_{13}** as its chloride salt by dissolving $Al(OH)_3 \bullet 0.7H_2O$ in 5 M HCl(aq). DLS data confirms the presence of near nanometer particles with an average hydrodynamic radius = 0.9 ± 0.1 nm, consistent with the nitrate analogue. Figure S1 shows the ^{27}Al NMR spectrum of the solution prepared by dissolution with HCl(aq) displays the same signals as the ***flat*-Al_{13}** prepared from nitric acid (see Figure 4.1.), without the small amount of Keggin impurity.

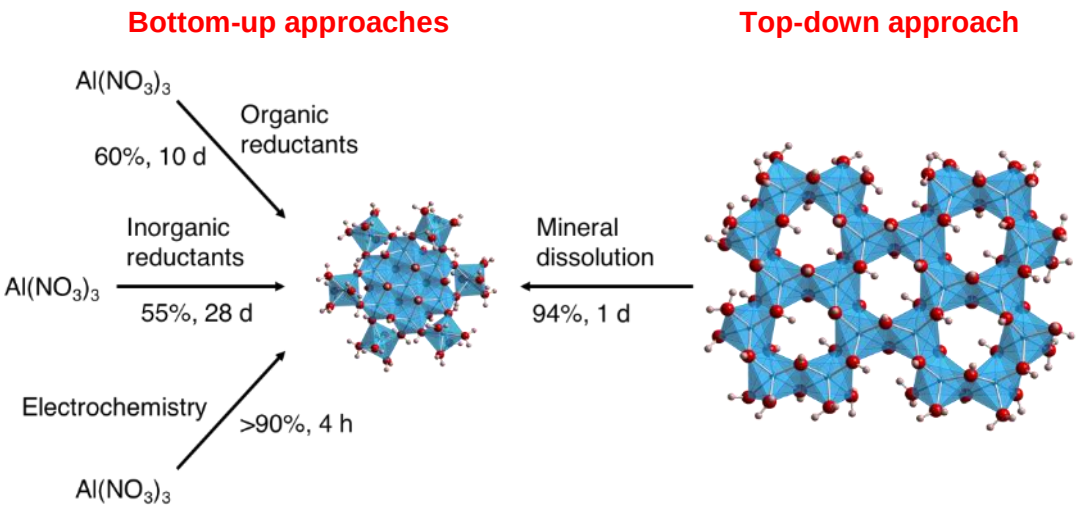

Scheme 4.1. Synthetic routes to produce the ***flat*-Al_{13}** cluster, showing the traditional bottom-up approaches and the method reported herein using a top-down approach from larger extended structures such as $Al(OH)_3$.

Previous syntheses of ***flat*-Al_{13}** require post-synthetic purification processes, or are restricted to small-scale reactions. The dissolution method requires no additional purification. To demonstrate scaling, we dissolved 181.1 g of $Al(OH)_3 \bullet 0.7H_2O$ in 2 L of 1.15 M HNO_3(aq) ($Al:NO_3$ = 13:15) in a 3-L round-bottom flask. After 24 h, the $Al(OH)_3 \bullet 0.7H_2O$ dissolved completely. All analyses of the reaction solution are consistent with our findings described above confirming ***flat*-Al_{13}** is the dominant species in the solution. The results highlight the high-level control of the synthetic method, even at a relatively large reaction scale (> 100 g of product).

Given the ability to scale and the potential low cost, we wanted to investigate the quality of the films produced with the as-prepared solution. To showcase the utility of the method, we studied solutions as precursors for deposition of Al_2O_3 films ranging from thick (> 100 nm) to ultrathin (4 nm) We focus on films deposited from the nitrate solution, though the Cl solution produces similar results.

We first prepared thick films to demonstrate our ability to build thick, uniform, films and to obviate difficulties related to characterizing ultrathin films. To build thick films, we deposited five successive coats with a 1-min cure at 230 ºC cure between each coat. Visually uniform, continuous thin films are readily deposited onto *p*-Si substrates from solutions of ***flat*-Al_{13}** with $[Al_{tot}]$ = 1.0 M. Here, we focus on films deposited from the ***flat*-Al_{13}** nitrate solution, though similar high quality films can be realized with the Cl containing solution as well. GIXRD patterns of films annealed up to 1000 ºC, show the amorphous nature of the film up to 700 ºC, evidenced by the lack of features in the diffraction pattern. For films annealed above 700 °C, the diffraction patterns show peaks consistent with crystalline γ-Al_2O_3 (Figure 4.3.).

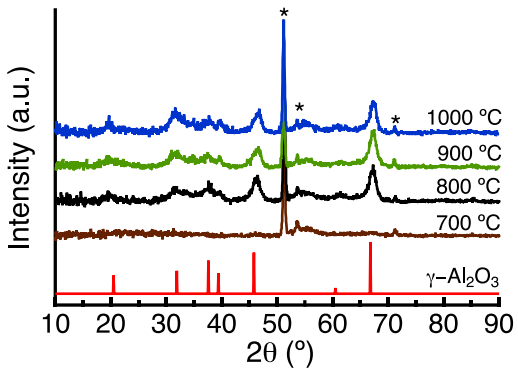

Figure 4.3. GIXRD patterns for alumina films after annealing at 700 (blue), 800 (red), and 900 ºC (black), referenced to γ-Al_2O_3 (green). * indicates peaks from *p*-Si.

We determined the index of refraction as a function of annealing temperature from analysis of spectroscopic ellipsometry data. Figure 4.4. shows Sellmeier fits of the dispersion curves and a general increase of refractive indexes with increasing annealing temperatures. After an initial 230 ºC cure for 1 min, films still contain substantial water, hydroxide, and nitrate counterions (Figure S2); these species elevate the polarizability and refractive index relative to films annealed up to 700 ºC, whereupon these species fully desorb. Increased film density drives the refractive index to higher values above 600 ºC. Alumina film have a refractive index near 1.64 (λ = 550 nm), when produced by atomic layer disposition (ALD).[24] Our films do not reach a comparable refractive index until annealed near 800 ºC. The data suggest solution-processed alumina films remain less dense than ALD deposited films up until their crystallization temperature (T ≈ 800 ºC). The lower densities of the solution-processed films likely result from the smaller coordination numbers of Al and O in the solution-processed films relative to those in ALD films, a result that stems from the unique reaction pathway of the solution precursor to the condensed solid. Simply, initial heating drives elimination of bound aqua ligands to low-coordination aluminum-centered polyhedral that share corners. These structural features differ

significantly from the six-coordinate and edge-sharing environments of dense Al_2O_3 corundum.

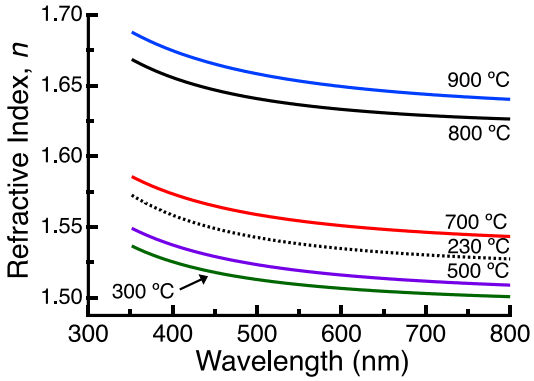

Figure 4.4. Modeled optical dispersion curves from the fit of the Sellmeier equation, $n^2(\lambda) = \mathrm{A} + \mathrm{B} \times \frac{\lambda^2}{\lambda^2 - \lambda_0^2}$, of the ellipsometry data.

The cross-sectional TEM images in Figure 4.5. reveal the ***flat*-Al_{13}** precursor produces a dense and continuous film, free of pores and voids. The image emphasizes a significant difference between cluster and other common routes for oxide film deposition: sputtered and conventional sol-gel methods for alumina deposition have produced films with rough and highly textured surfaces.[25–28] Moreover, the TEM images exhibit sharp, smooth interfaces with the carbon protecting layer, once again demonstrating the exceptional quality of the film. To emphasize the surface smoothness, we measured a root-mean-square roughness of ~0.3 nm with AFM on a sample annealed at 500 ºC for 1 h (Figure S3).

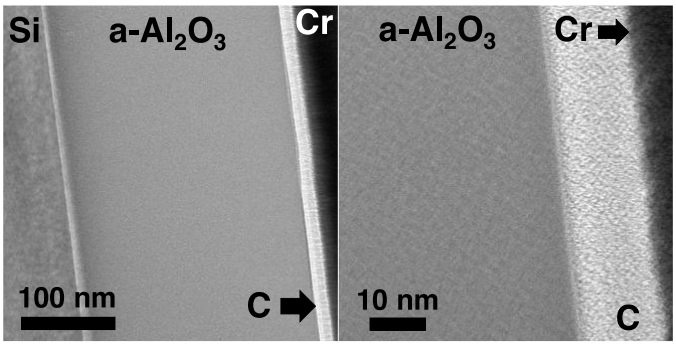

Figure 4.5. Cross-sectional TEM image of a 247-nm amorphous-Al_2O_3 (a-Al_2O_3) film annealed at 500 ºC (left) and an image of the same film with increased magnification at the interface between C and the a-Al_2O_3 thin film (right).

Next, we investigated the deposition of thinner films (< 50 nm) by diluting the stock solution to selected [Al_{tot}] concentrations in the range 0.1 to 1.0 M, casting the solution of *p*-Si substrates, then annealing at 500 °C for 1 h. Figure S4 shows the linear relationship between solution concentration and film thickness, determined from ellipsometry data. Eq. 1 summarizes quantitatively the relations film thickness, *t*, and Al molarity, *c*:

$$t = \left[41.0c\ \mathrm{M}^{-1}\right]\ \mathrm{nm} \quad (1).$$

Across the studied concentration range, thickness may be tuned from 4.0 to 41 nm by setting the [Al_{tot}] between 0.1 and 1.0 M (Figure S4).

Figure 4.6. shows the current-voltage (I-V) characteristics of metal-insulator-semiconductor (MIS) test structures constructed with Al_2O_3 films heated between 350 and 700 ºC. Table 1 summarizes results. Here, we consider only the negative-bias data. They represent injection from the aluminum top contact, therefore, contributions from traps or non-idealities at the Al_2O_3/ SiO_2 interface should be minimal. The leakage current density at -1 MV/cm (*Jleak*) is consistently near 10 nA/cm^2 for Al_2O_3 films annealed above 350 ºC (Table 1). The drop in leakage current density, from 148 nA/cm^2 at 350 ºC to 9.8 nA/cm^2 at 500 ºC, is likely due to loss of hydroxide. We note the J-E curve of the film annealed at 700 ºC shows behavior that mimics SiO_2, with a knee in the curve at a field of ~5.5 MV/cm. Growth of interfacial SiO_2 is expected for aqueous-solution-processed alumina, and high temperature anneals accelerate the growth.[13] We found the relative dielectric constant (ε_r) for films annealed over the range 350–500 ºC to be approximately 5.9. We attribute the near constant ε_r to the loss of a large fraction of polarizable hydroxide groups and nitrate counterions below 350 ºC. The drop in ε_r at 700 ºC is again consistent with the growth of interfacial SiO_2, as ε_r for SiO_2 is 3.9. Because of the work-function difference of ~0.9 eV

between Al and *p*-type Si, positive bias breakdown fields are lower than those for negative bias. Thus, positive breakdown fields are a conservative estimates of breakdown strength. A large breakdown field of > +6 MV/cm is observed for films annealed as low as 350 ºC, increasing to > +7 MV/cm at 500 ºC and higher temperatures.

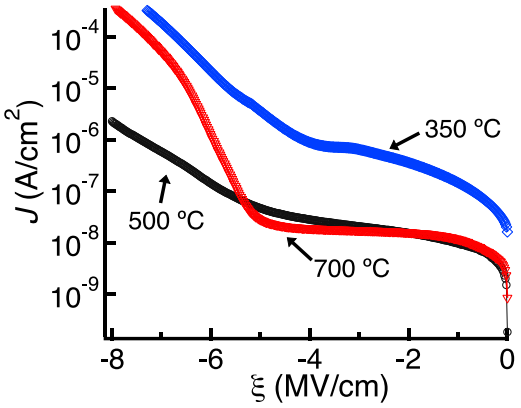

Figure 4.6. Characteristic J-E curves for solution processed a-Al_2O_3 thin films annealed at 350 (blue), 500 (black), and 700 ºC (red).

Temperature (ºC)	Thickness (nm)	J_{leak} (nA/cm^2)	ε_r	Average Breakdown (MV/cm)
350	27.5	148.4	5.8	6.6 ± 0.5
500	24.5	9.8	5.9	7.6 ± 0.4
700	22.7	11.9	4.9	7.3 ± 0.6

Table 4.2. Summary of Electrical Results for MIS Test Structures.

Other researchers have deposited films from simple $Al(NO_3)_3$ salt solutions with a various degrees of success.[29–31] For example, $Al(NO_3)_3$ dissolved in ethanol produces highly textured films, as observed by AFM surface imaging.[29] This texture is likely associated with crystallization that occurs as the $Al(NO_3)_3$ precursor dries during spin coating. We do not observe this effect for the ***flat*-Al_{13}** precursor, which because its bulky

size and high hydration level is more difficult to crystallize. Further, we find many simple salt solutions, including $Al(NO_3)_3$(aq), produce discontinuous and nonuniform films, especially for multiple-coat depositions. Branquinho and co-worker describe similar observations, wherein $Al(NO_3)_3$-urea combinations for "combustion" reactions produce discontinuous films.[31]

4.4. CONCLUSION

We have shown that a common aluminum mineral dissolves in acid to produce an aqueous aluminum precursor that forms high-performance oxide thin films. Since only HNO_3(aq) and $Al(OH)_3$ react stoichiometrically to produce the precursor, no post-synthesis purification is needed. The approach is atom efficient, as it forms only small amounts of H_2O as a byproduct. Overall, the method is simple and scalable, and it provides a route to high-purity products. It is significantly more practical than methods previously reported to prepare ***flat*-Al_{13}**. The precursor enables deposition of films with reproducible thicknesses by changing solution concentration and applying multiple spin coats. Film dielectric constants and leakage currents compare to those previously reported for films deposited from precursors prepared by the Zn-metal route. Overall, the method is simple and scalable, and it provides a route to high-purity thin films of interest for electronics, optics, and optoelectronics.

4.5. CHAPTER V BRIDGE

While the dissolution approach pathway has focused on aqueous aluminum chemistry, chapter 5 is designed to showcase how this approach can be applied across the periodic table to other metal systems. Chapter 5 focuses on the aqueous chemistry of

scandium oxo-hydroxo species, particularly the scandium dimer having the formula $[Sc_2(\mu\text{-}OH)_2(H_2O)_6(NO_3)_2](NO_3)_2$ (**Sc_2**). Using ^{45}Sc NMR in a similar way in which ^{27}Al NMR was used to identify aluminum speciation has helped us to begin to understand scandium speciation.

CHAPTER V

SYNTHESIS AND CHARACTERIZATION OF AQUEOUS INORGANIC SCANDIUM OXO-HYDROXO SPECIES

5.1 INTRODUCTION

My contributions to this work included experimental design and synthesis as well as characterization techniques to observe the $[Sc_2(\mu\text{-}OH)_2(H_2O)_6(NO_3)_2](NO_3)_2$ cluster in the solution state. Using the dissolution pathway approach, single crystals of the $[Sc_2(\mu\text{-}OH)_2(H_2O)_6(NO_3)_2](NO_3)_2$ cluster were isolated for analysis. I also utilized ^{45}Sc nuclear magnet resonance (NMR) imaging to determine aqueous speciation changes as a function of concentration and pH. Dr. Michael Strain and Dr. Nanette Jarenwattananon aided in this work by assisting with the ^{45}Sc NMR pulse program sequence. Dr. Cory Perkins aided in this work by using computational methods in the gas phase to determine the expected ^{45}Sc NMR peak shifts of the $[Sc_2(\mu\text{-}OH)_2(H_2O)_6(NO_3)_2](NO_3)_2$ cluster using density functional theory (DFT). Elizabeth Cochran assisted in this work by performing precursory thin film experiments from the solution precursors for scandium oxide (Sc_2O_3) thin films. The techniques used for Sc_2O_3 thin film formation involved an all aqueous solution processing method and techniques used to analyze film quality included Infrared (IR) spectroscopy. Dr. Lev N. Zakharov collected all single crystal X-ray diffraction data. The results presented herein are unpublished at this time but would be ideal for the journal *Inorganic Chemistry*.

Transparent electronics and devices are continuously emerging to create the next generation of technological advancements. This is due, in part, to the fairly accurate

prediction Moore's Law made decades ago in relationship to the growth rate of the transistor.[1] Scandium oxide (Sc_2O_3) has gained attraction as a high-k dielectric material due to having a band gap of 5.7 eV. [2–4] This wide band gap material has commercial use cases in high powered lasers, mercury lamps, and the aerospace industry as scandium is known to form alloys with aluminum mineral structures.[5,6]

Here we present a process that yields the obscure oxo-hydroxo cluster $[Sc_2(\mu\text{-}OH)_2(H_2O)_6(NO_3)_2](NO_3)_2$ (**Sc_2**) (Figure 5.1) by a dissolution approach of $Sc(OH)_3$ in the presence of HNO_3. While single crystals were isolated from the reaction mixture the solution is not stable for a prolonged period of time. To the best of our knowledge this is only the second instance in which the all inorganic **Sc_2** cluster has been synthesized containing nitrate-coordinating anions. This dissolution approach was inspired by a similar dissolution method used to differentiate between aluminum based oxo-hydroxo clusters.[7]

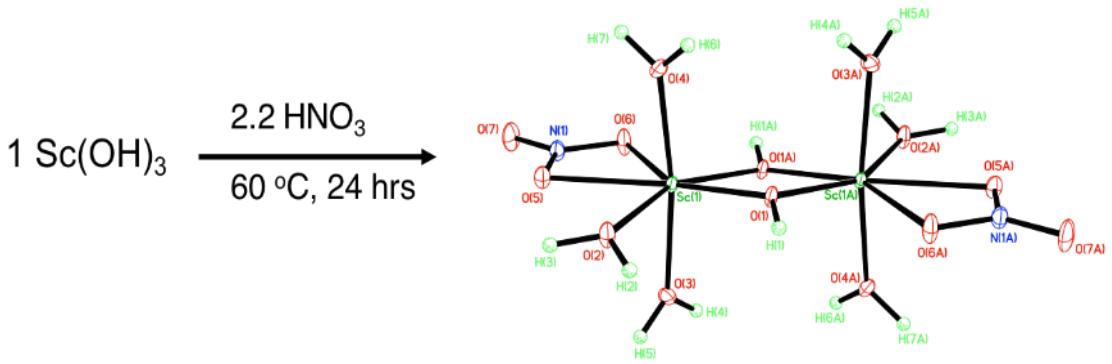

Figure 5.1. A simple synthesis of the dissolution of $Sc(OH)_3$ with HNO_3 to form **Sc_2**. The reaction mixture was then stirred and heated at 60 °C for 24 hours. Sc^{3+} ions (green) are hepta-coordinate in the above crystal structure. The two non-coordinating nitrates have been omitted from the wireframe structure for clarity.

The rare earth metal scandium was discovered in 1879 and gets its namesake from the European country Scandinavia. Scandium saw its first commercial use cases during World War II when the Soviet Union found it enhanced the strength and lowered the weight of current aluminum based fighter jets. This is due to scandium's ability to form alloys with aluminum mineral based architectures, meaning that scandium can be substituted into the crystal lattice site of bulk aluminum structures. As a d^0 metal its chemical properties range between that of traditional rare earth metals and the Group 13 block elements.[8] Scandium is only observed in the 3+ oxidation state and has aqueous hydrolysis products existing in the pH range of ~1-4. Beyond this pH range insoluble $Sc(OH)_3$ products begin to precipitate. Due to these characteristics scandium is thought to behave similarly to aluminum at low pH regimes. However, unlike aluminum, which is amphoteric and has additional soluble hydrolysis products at basic conditions (~pH 9), $Sc(OH)_3$ products do not re-dissolve under basic conditions except for the scandiate ion Sc(OH)4-, which is believed to persist as supported by its Pourbaix diagram (Figure 5.2).

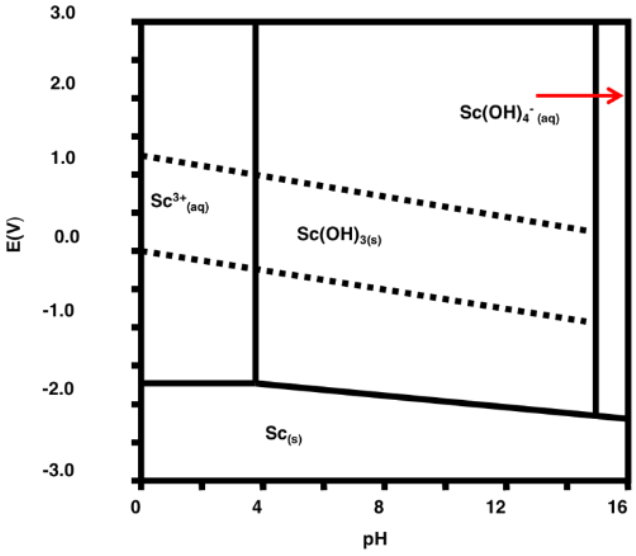

Figure 5.2. Pourbaix diagram of scandium.

Early scandium aqueous speciation research dates back to the mid 1950's when Kilpatrick and Pokras were interested in the acid dissociation of aquoscandium ions. This work inspired new aqueous scandium research into the 1980's.[9,10,11,12] Originally, it was believed that only a handful of scandium oxo-hydroxo species exist before precipitation of insoluble $Sc(OH)_3$. Of these species only a handful have been isolated with a known crystal structure and chemical formula, and for the most part have been some derivatized version of the **Sc_2** dimer cluster. The **Sc_2** cluster has been reported a handful of times with large organic coordinating ligands, generally with crown either motifs as reported by Webster and co-workers.[13,14] These types of ligands have been known to help influence structure coordination and enhance crystallization as opposed to analogs with completely inorganic based ligands. In addition to **Sc_2** dimer clusters made with bulky organic ligands there has been efforts to show the coordination with halides as well. Webster et al. were able to substitute on the complex $[Sc_2(\mu\text{-}OH)_2(H_2O)_6X_4]$ where X = Cl, I, or Br .[11] This work inspired the more recent studies done by Wei Wang and co-workers.[15] In this result an all inorganic $[Sc_2(\mu\text{-}OH)_2(H_2O)_6(NO_3)_2](NO_3)_2$ structure was prepared via a Zn reduction synthetic method. Protons and nitrates are reduced which drives olation, leading to an increase in pH and formation of larger oligomers. This work showcased one of few all inorganic **Sc_2** dimer clusters but also built upon a similar synthetic method that had been previously shown to isolate the larger Group 13 oxo-hydroxo clusters **Al_{13}** and **Ga_{13}**. Unlike the **Al_3** and **Ga_{13}** clusters which display non-coordinating nitrate anions, the **Sc_2** dimer cluster contains both inner sphere (two) and outer sphere (two) nitrate anions.

Th Sc_2 dimer cluster presented here is only the second report of this cluster type having an identical crystal structure and chemical formula to what was observed in Wei

Wang's work. However, the dissolution method is an enhancement over the Zn reduction synthesis which was produced at 65% yield and still required a post-purification step to remove excess $Zn(NO_3)_2$ by an isopropanol wash of the crystals. The dissolution approach requires no post-purification step and has the potential to be a scalable precursor for future Sc_2O_3 materials and thin films.

Polynuclear NMR has seen great advancements since the early days of scandium chemistry in the mid 1950's and can now be employed to better understand Sc speciation. The metal nucleus ^{45}Sc has an abundance of 100% making it a practical technique to better understand scandium species. Unfortunately, its 7/2 spin state and quadropolar nature makes it difficult to definitively understand chemical shifts within the NMR spectra. In this study it is suggested that we may have found by ^{45}Sc NMR the first known report of the chemical shift corresponding exactly to the **Sc_2** dimer cluster. The base addition route presented herein also suggests a way to study the evolution of speciation as a function of pH, while the dissolution approach pathway does not.

5.2. EXPERIMENTAL

5.2.1. General Methods. All reagents were purchased from commercial grade sources and used as received. Scandium nitrate (hydrated) (99.9%), nitric acid, and sodium hydroxide pellets were purchased from Sigma-Aldrich Corporation. 18.2 (MΩ) water was used in all experiments unless otherwise stated. Unless specified, all reactions for the dissolution method were conducted in 50 mL centrifuge tubes then converted to 20 mL scintillation vials. All base addition with sodium hydroxide experiments were conducted in 20 mL scintillation vials. ^{45}Sc and ^{1}H NMR spectra were collected on a Bruker 600 MHz

NMR spectrometer. pH measurements were taken to find that solutions exist in the range of 1.7-4.1.

This chapter describes a $[Sc_2(\mu\text{-}OH)_2(H_2O)_6(NO_3)_2](NO_3)_2$ (**Sc_2**) cluster is synthesized through a dissolution of $Sc(OH)_3$ in the presence of a strong acid (HNO_3). As evaporation occurred over several months, flat plate-like crystals were isolated from the reaction mixture and analyzed in the solid state using single crystal X-ray diffraction (XRD) to determine a crystal structure and chemical formula consistent with **Sc_2**. Thin films of scandium oxide were prepared from both dissolution and base addition methods and at this time a stable Sc solution precursor is still needed to make high quality Sc_2O_3 thin films.

5.2.2. General Procedure for the synthesis of Sc_2 via a dissolution method. A 0.5M aqueous solution of $Sc(NO_3)_3$ (10 mL) was sonicated for 10 min. in a 20 mL scintillation vial allowing for the metal salt to completely dissolve. The solution was then transferred to a 50 mL centrifuge tube and an excess amount of NaOH was added to completely precipitate $Sc(OH)_3$. The reaction mixture was then centrifuged at 7500 rpm for 20 min. and aqueous $NaNO_3$ was decanted from the insoluble $Sc(OH)_3$ filtrant. The filtrant was washed with water 5 times then a 2.2 molar ratio ($Sc:NO_3$) of HNO_3 was added to the filtrant dissolve $Sc(OH)_3$. This reaction mixture was transferred back to a 20 mL scintillation vial and heated at 60 ºC for 24 hours and displays a cloudy solution, as not all Sc is dissolved. Next the reaction mixture was transferred to a test tube where over the course of many months small plate-like crystals of **Sc_2** formed.

5.2.3. General Procedure for synthesis of Sc_2 and Sc oxo-hydroxo species via a base addition method. A 0.5M aqueous solution of $Sc(NO_3)_3$ (10 mL) was sonicated for 10 min. in a 20 mL scintillation vial allowing for the metal salt to completely dissolve. Then the slow addition of NaOH at a tunable addition rates ranging from 0.125-3 mol ratio (Sc:Na) was added to the reaction mixture. These reaction mixtures were not isolated for single crystal but used solely in the solution state. This identical procedure was used substituting NaOH for NH_4OH as well.

5.2.4. General Procedure for computational calculation of Sc2 dimer. We employ Density Functional Theory (DFT) was to model the local structures and 45Sc NMR chemical shifts of scandium compounds using Gaussian 09 software. Here, we use the hybrid functional PBE02 and Pople basis sets. The combination of PBE0/6-311G** was used to optimize gas-phase structures and PBE0/6-311++G** level for NMR shifts.

Grazing incidence X-ray diffraction (GIXRD) was performed on three-layer films using a Rigaku SmartLab diffractometer with a Cu Kα radiation source (λ_{avg}=1.5418 Å, Ni foil Kβ filter), using a 0.5° incident beam angle, 0.1° step size, and 30s integration at each step. Films for XRD were first soft-baked at 125 °C for 5 min, then ramped to the final annealing temperature (12.5 °C min^{-1}) and held for 1h.

Sc_2O_3 Films for Fourier-transform infrared spectroscopy (FTIR) were deposited on double-side polished p-type Si substrates. Spectra were collected using a Thermo Fisher Nicolet 6700 spectrometer in transmission mode. Background correction was accomplished using bare Si with the same thermal history as the film. A single film spun

from a 0.75M $Sc(NO_3)_3$ solution was annealed at each temperature step for 5 min before each spectrum was collected.

5.3. RESULTS AND DISCUSSION

Cluster synthesis and characterization. The ^{45}Sc NMR spectra of the simple monomer $Sc(NO_3)_3$ reveals a single chemical shift at 3.97 ppm (Figure 5.3.). This is fairly consistent to what has previously been reported. In previous reports it has been shown that a scandium monomer species can see a slight chemical shift just as a function of concentration. That is to be expected here as the sample is only 0.5M with respect to Sc^{3+}. Increasing the Sc^{3+} concentration or lowering solution pH further with HNO_3 would lead to a slight shift towards 0 ppm.

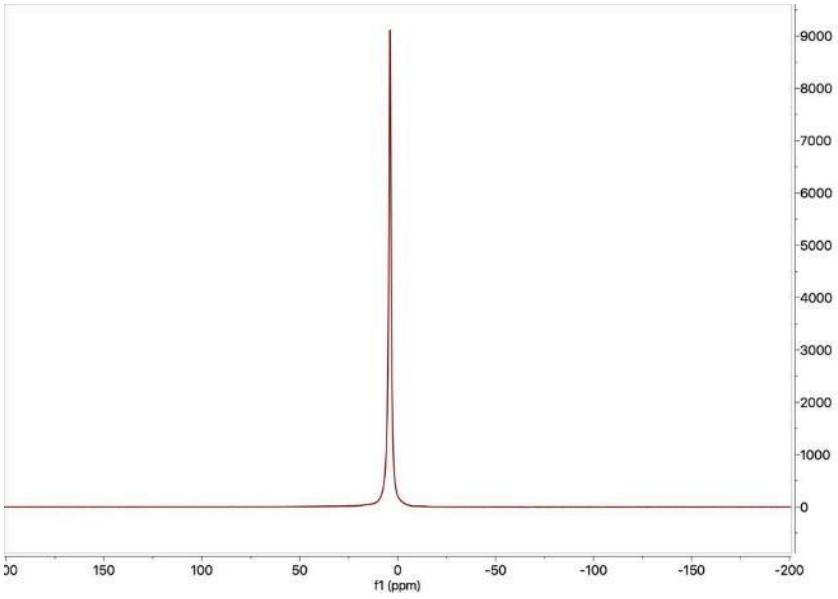

Figure 5.3. ^{45}Sc NMR spectra of the $Sc(NO_3)_3$ monomer at 0.5M with respect to Sc^{3+}. The spectra was collected in a 90%/10% H_2O/D_2O ratio on a 600 MHz Bruker NMR spectrometer. The observable chemical shift is at 3.97 ppm.

To further understand the speciation and hydrolysis of products of scandium the slow addition of base was added to several $Sc(NO_3)_3$ solutions with increasing basicity from 1.7-4.1. The base was added in a molar ratio of 0:2 with respect to Sc^{3+}:Na content (Figure 5.4.). It was observed that with increasing base the original chemical shift of the $Sc(NO_3)_3$ monomer at 3.97 shifted downfield to higher ppm, it can be observed at 14.5 ppm in the most basic solutions. This shift from a narrow intense monomer peak suggests that larger scandium oxo-hydroxo species form under more basic conditions which is expected by speciation and Pourbaix diagrams for scandium (figure 5.2.). The line broadening of this peak also leads us to believe the speciation is transitioning away from the highly symmetric scandium monomer to more asymmetrical species with increased basicity. Additionally, a downfield peak arising at 42.5 ppm increases with increased basicity. It is also expected that this species is a fragment of higher order scandium clusters and could potentially be a unit contained within Sc_2 or a larger scandium oxo-hydroxo species.

To better understand the slow addition of base to the $Sc(NO_3)_3$ monomer solution NaOH was replaced with a slightly weaker base, NH_4OH. Unlike NaOH which is expected to completely dissociate in water, NH_4OH does not. Na^+ ions were expected to be non-coordinating in solution and not participate in binding during the formation of scandium oxo-hydroxo species. However, because NH_4OH is a weaker base than NaOH, and appreciable amount of NH_3 is present which may have a higher affinity for coordination and may in fact compete with scandium oxo-hydroxo cluster binding. This can be hypothesized based on ^{45}Sc NMR spectra (Figure 5.5.) collected under identical molar ratios for the two bases with respect to scandium (1:1).

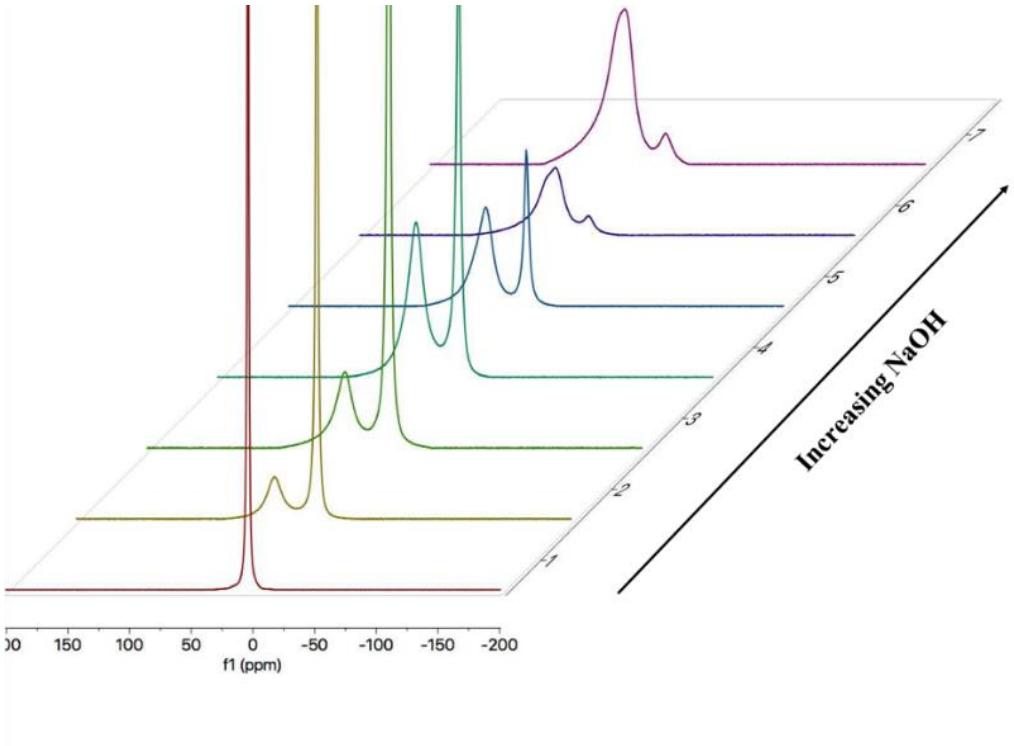

Figure 5.4. ^{45}Sc NMR of stacked plot from base addition with increasing NaOH in a molar ratio ranging from 1:0 to 1:2 with respect to Sc^{3+}:Na^{+} content. The solution NMR was carried out in a 90%/10% H_2O/D_2O mixture at room temperature. A decay of the original monomeric chemical shift at 3.97 ppm can be observed while an increase in intensity can be observed for a chemical shift arising at 42.6 ppm.

While the sample in red from base addition with NaOH shows a lower intensity and more narrow line shape for the peak at 42.5 ppm the solution from NH_4OH addition shows a broader line shape and much more intense peak at 42.5 ppm and a decreased monomer peak relative to each spectra at elevated base addition. This may suggest that NH_3 binds directly to form larger order scandium hydroxo- clusters more rapidly than does NaOH.

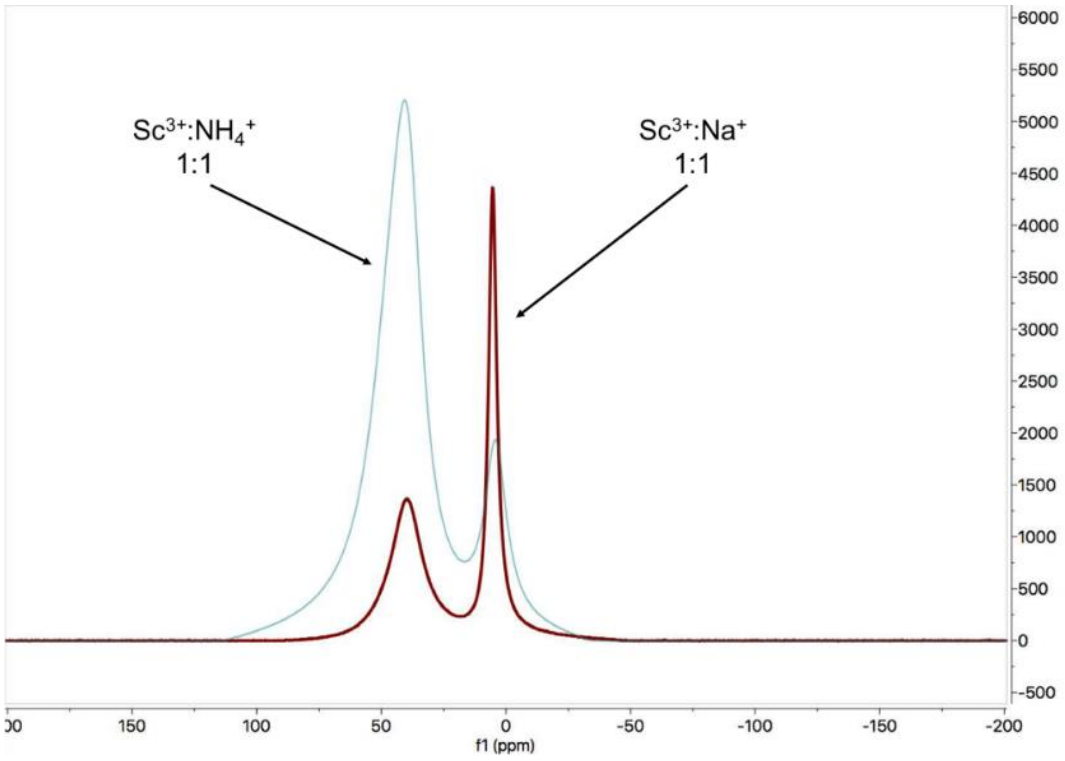

Figure 5.5. ^{45}Sc NMR of a base addition method comparing NaOH to NH_4OH under identical molar ratios. Each solution is 1:1 with respect to Sc^{3+}content. The solution NMR was carried out in a 90%/10% H_2O/D_2O mixture at room temperature. NaOH (red) shows a narrow intense chemical shift ~9 ppm while the NH_4OH solution (blue) shows a broader and decaying chemical shift in the same region.

Thin Film Studies. Scandium oxide (Sc_2O_3) thin films from a Sc(NO3)3 monomer solution were soft-baked at 125 ^oC then annealed at increasing temperatures ranging from 200-500 ^oC. The thin films are amorphous at low temperatures and do not seem to reach crystallinity until elevated temperatures upwards of 400 ^oC.

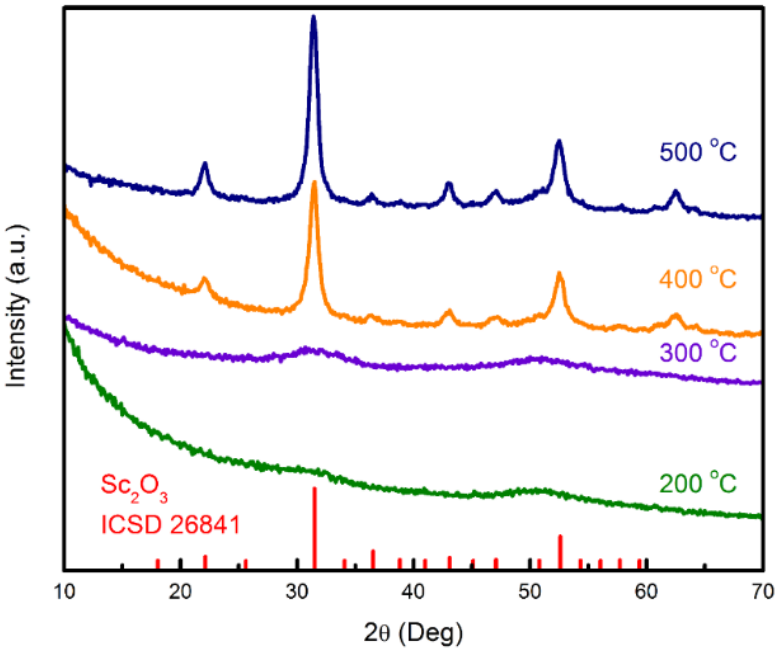

Figure 5.6. GIXRD of Sc_2O_3 thin films at increasing annealing temperatures. The thin films do not begin to show crystallinity until elevated temperatures around 400 °C.

FTIR was also used to show the decaying nitrate stretches in the Sc_2O_3 films at increasing annealing conditions ranging from 50-500 °C. As the annealing temperature increases from 50-500 °C, nitrate and hydroxyl groups are continually removed. After 400 °C, nitrate and hydroxyls are no longer present, indicating complete condensation to the oxide.

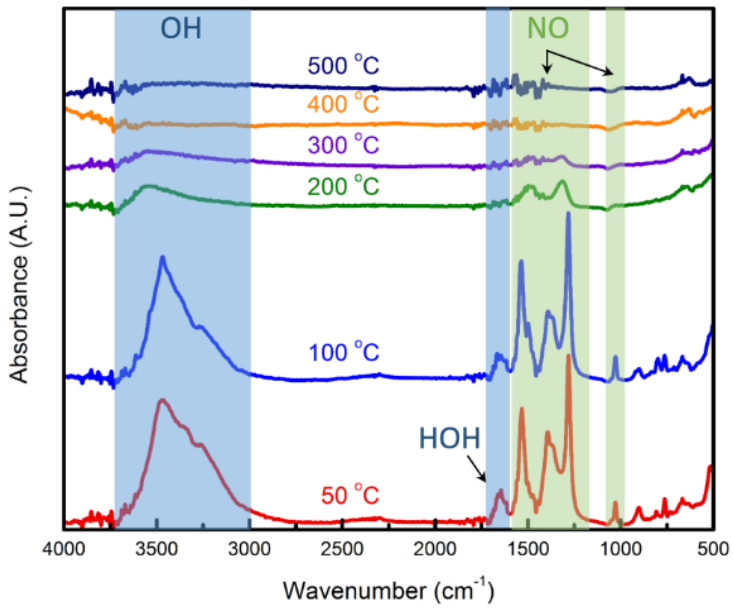

Figure 5.7. FTIR spectra of $Sc(NO_3)_3$ at increasing annealing temperatures ranging from 50-500 °C. At elevated temperatures above 400 °C nitrates and hydroxyls are no longer present.

5.4. CONCLUSIONS

In summary, we have been able to synthesize the all inorganic **Sc_2** dimer cluster via a dissolution method. ^{45}Sc NMR via a base addition showcases evolution of scandium hydrolysis products and reveals that the solution state characteristics suggest that the species are in a dynamic equilibrium. Solutions made with NaOH and NH_4OH at the same concentration reveal different distribution of products based on intensity. This suggests that Na^+ bonds in a non-coordinating fashion, differently than NH_3 or NH_4^+, as one of the species could be bonded directly to the Sc oxo-hydroxyo species through coordination or hydrogen bonding, thus creating an entirely different chemical species and resultant chemical shift. Computational studies done to predict the exact chemical shift of **Sc_2** detail that there should be only one chemical shift as both scandium ions within Sc_2 are

isoelectronic. There exists a distinct chemical shift for the $Sc(NO_3)_3$ monomer in relation to what is expected for larger oligomeric species including the **Sc_2** dimer. Preliminary Sc_2O_3 thin film studies from a $Sc(NO_3)_3$ monomer solution give promise to how these precursors can be used for future solution processed methods. In future work we would like to employ thin film studies from a stable **Sc_2** precursor solution to thin film materials.

5.5. CHAPTER VI BRIDGE

While aqueous scandium speciation is still being expanded upon with ^{45}Sc NMR spectroscopy and related solution based techniques, there is still a need to improve fundamental solid state characterization for scandium materials as well. For instance, a need for greener solution processing methods of aqueous Sc_2O_3 thin films will be needed as these materials see more potential applications. Sc_2O_3 is an dielectric thin film material due to its wide band gap of 6 eV. As semiconductor and aerospace industries see growth in coming years, the need for better materials can be expected and Sc_2O_3 could be a viable candidate based on its wide band gap. The next chapter takes us to the conclusion of this thesis work. It is meant to highlight how the solution studies and behavior of metals Al^{3+} and Sc^{3+} give rise to information on their solution speciation and will aid in identifying new cluster types.

CHAPTER VI

CLOSING REMARKS

Within the scope of my thesis research I was able to make great contributions toward understanding aqueous aluminum speciation. The synthetic top down dissolution approach pathways employed to better understand aluminum cluster speciation expanded on the previous bottom up approaches set forth by my colleagues and literature reports. These results were able to showcase the robustness of ^{27}Al NMR spectroscopy in the solution state and may lead to new breakthroughs in finding the next generation of aluminum cluster species. As scientists continue to advance new solution and solid state characterization methods at the nanoscale level it will allow for the identification of new species. It is my hope that the work presented herein will help those discoveries become easier through my contributions to the field. Nanoscale clusters will continue to be a great candidate for metal oxide thin film precursors and this work is just a snapshot of how the cluster toolbox can be expanded to potentially create new materials. As polynuclear NMR spectroscopy continues to develop understanding of the speciation of difficult nuclei such as scandium, gallium, and indium there will be new opportunities to connect solution and solid state chemical properties. In the year 2019, as a society, we are more technologically advanced than we have ever been and I am excited to see how aqueous cluster chemistry will grow. Though I was not able to solve every problem related to aluminum speciation, I hope I added to the great science that has been done in this space and I look forward to how future researchers may take my studies and expand upon them in future offerings.

APPENDIX

SUPPLEMENTAL INFORMATION

CHAPTER II SUPPLEMENTAL INFORMATION

Experimental

We prepared solutions by dissolving $Al(OH)_3 \bullet 0.7H_2O$ (Alfa Aesar) in H_2SO_4 (aq) (Mallinckrodt) with an $Al:SO_4^{2-}$ ratio of 1:1. After adding the $Al(OH)_3 \bullet 0.7H_2O$, the slurry was stirred under mild heat (70 ºC) overnight to produce a colorless solution. Similarly, we prepared a solution by dissolving $Al(OH)_3 \bullet 0.7H_2O$ in an aqueous solution of $Al_2(SO_4)_3 \bullet 18H_2O$ (J. T. Baker), with an $Al:SO_4^{2-}$ ratio of 1:1. We dissolved $Al(OH)_3 \bullet 0.7H_2O$ in 40% wt H_2SeO_4 (aq) to produce solutions with $Al:SeO_4^{2-}$ ratios of 1:1.4 and 1:1. Solutions of $[Al_{tot}] = 3$ M were prepared with $Al:SO_4^{2-}$ and $Al:SeO_4^{2-}$ ratios of 8:5 and 8:6, respectively; the $Al(OH)_3 \bullet 0.7H_2O$ starting material was less soluble in H_2SeO_4 (aq) than in H_2SO_4 (aq).

Single crystals grew via slow evaporation in open scintillation vials, typically forming within 2 weeks. They were isolated from the mother liquor, immediately coated in oil, and placed on a Bruker D8 Quest X-ray diffractometer equipped with Mo Kα radiation (λ = 0.71017 Å), a CMOS detector, and an Oxford Cryosystems Cryostream 800 low-temperature attachment. Data were collected at 100 K. Crystals from dissolution in $Al_2(SO_4)_3 \bullet 18H_2O$ and H_2SO_4(aq) have triclinic cells represented by the unit-cell parameters a = 9.218(2) Å, b = 12.002(2) Å, c =14.618(3) Å, α = 99.878(7)°, β = 102.863(6)°, γ = 110.204(5)°, and V = 1424.1(4) Å^3. These parameters, as well as refined

atomic parameters, match the crystallographic results reported previously for $[Al_8(\mu_3\text{-}OH)_2(\mu_2\text{-}OH)_{12}(H_2O)_{18}](SO_4)_5 \bullet 16\ H_2O$.[1] Crystals isolated from H_2SeO_4(aq) were determined to be $Al_2(SeO_4)_3 \bullet 4.5\ H_2O$, a structure that has not previously been reported.

Composition was determined thermal gravimetric analysis using a Q50 TGA analyzer (TA instruments). To complement the TGA, crystals were dissolved in HNO_3 and SO_4^{2-} content was determined by quantitative gravimetric analysis by adding $BaCl_2$ and precipitating $BaSO_4$. The resultant solution was boiled for 5 min and left at 80 ºC for 12 h to facilitate quantitative precipitation.[2] The precipitate was washed until the filtrate was no longer precipitated AgCl with addition of $AgNO_3$.

Prior to thin-film deposition, substrates were treated in a low-energy O_2 plasma to create a clean, hydrophilic surface. The films were deposited onto 100-nm thermally grown SiO_2/Si. Films were deposited by spin coating the aqueous **Al_8** precursor at 3000 rpm for 30 s. After deposition, the films were cured at 300 °C for 1 min and then annealed to 500 ºC. Top-down and cross-sectional SEM images of thin films were collected on a FEI Helios 650 dual beam SEM.

^{27}Al NMR spectra were collected on a Bruker 400-MHz DPX-400 Spectrometer with samples in a 90% H_2O-10% D_2O solution. An insert containing $NaAl(OH)_4$ (0.04 M) served as an internal standard in an external coaxial glass NMR insert for determination of chemical shifts and intensities.

Small and wide angle X-ray scattering data were collected on an Anton Paar SAXSess with Cu-Kα radiation (λ =1.54 Å) and a 2-D image plate detector with a sample-to-image-plate distance of 26.1 cm. Data were collected with line collimation over the q range 0.018-2.5 $Å^{-1}$. Solutions were contained in 1.5-mm borosilicate glass capillaries and

exposed to X-rays for 30 min. Data were collected and initially process with the SAXSquant software package. Data were analyzed with Igor Pro software and Irena macros.[3] SolX[4,5] software produced simulated scattering curves from the structural data described above.

ESI-MS measurements were made with an Agilent 6230 ESI-MS system comprising a Time-of-Flight (TOF) mass spectrometer coupled to an electrospray ionizer. 10-μL volumes of the as-prepared solutions ($[Al^{3+}]$ = 0.1-0.2 M) were first mixed with water, then injected into the ESI-MS system with an Agilent 1260 Infinity quaternary pump at a flow rate of 0.4 mL min^{-1}. Solutions were nebulized with the aid of heated N_2(g) (325 ºC) flowing under a pressure of 35 psig (241 kPa) at 8 L min^{-1}. Voltages of the capillary, skimmer, and RT octopole were set at 3500, 65 and 750 V, respectively, while the voltage of the fragmenter was set at 100 V. The data were collected in negative ion mode.

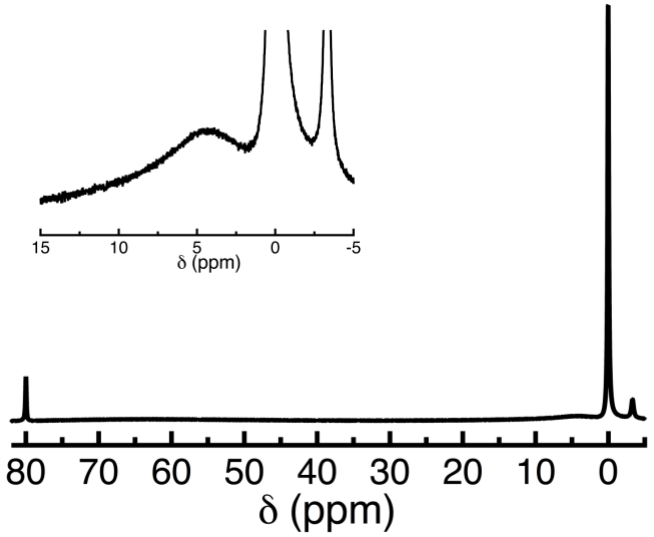

Figure S1: ^{27}Al NMR spectrum of the cluster containing solution ($[Al_{tot}]$ = 1 M). The inset highlights the spectral region of six-coordinate aluminum.

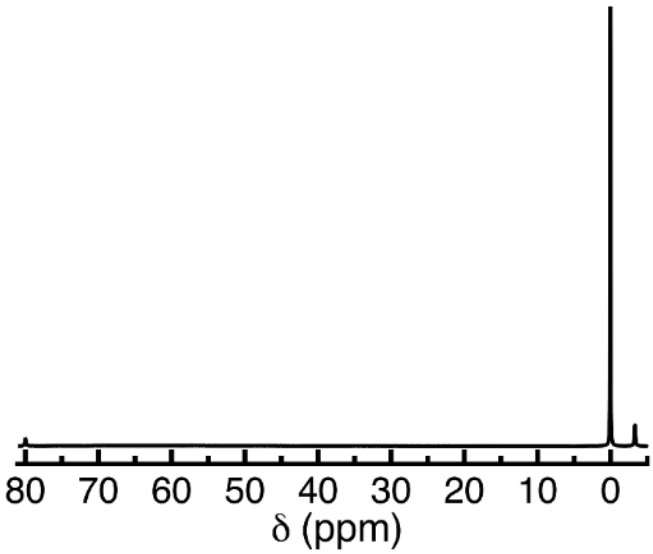

Figure S2. ^{27}Al NMR spectrum of 0.5-M $Al_2(SO_4)_3$ solution (1 M Al^{3+})

Table S1. Signal intensities divided by the internal standard.

Signal (ppm)	1 M Al_8	3 M Al_8	0.5 M $Al_2(SO_4)_3$
0	11.94	9.47	24.64
-3.3	1.08	0.50	2.92

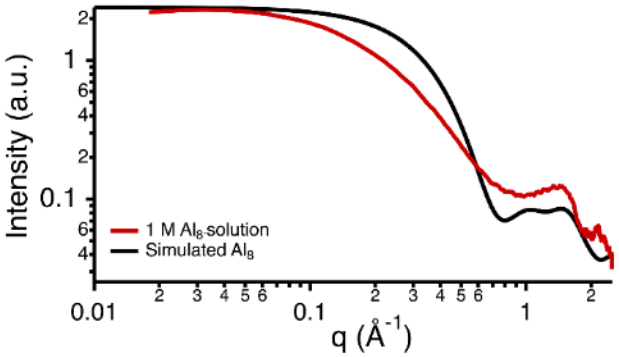

Figure S3. SWAXS curve of the as-prepared [Al_{tot}] = 1 M solution containing and simulated **Al_8** curve. Data are normalized for ease of comparison.

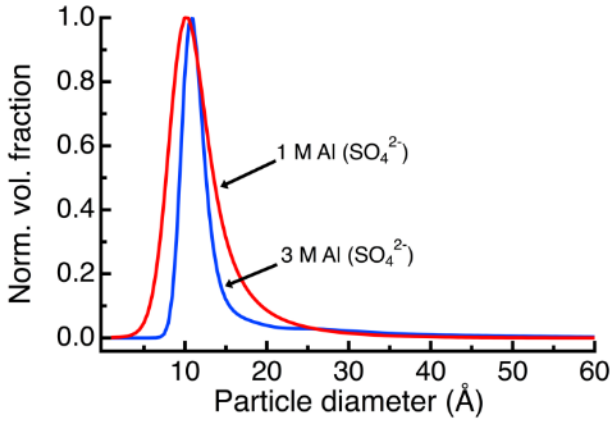

Figure S4. Particle size distribution analysis of the SWAXS data of the 1-M (red) and 3-m (blue) reaction mixtures.

Solution	Diameter (Å)	FWHM	Peak area (%)
1 M reaction solution	10.1	5.0	74
	14.5	9.1	36
3 M reaction solution	10.7	2.7	62
	12.8	2.3	22
	20.7	17.3	16

Table S2. Gaussian peak fitting of size distribution analysis.

Composition	m/z (measured)	m/z (calculated)
$[H_3(SO_4)_2]^-$	194.9289	194.9275
$[Al(SO_4)_2]^-$	218.8877	218.8855
$[Al_2(OH)_3(SO_4)_2]^-$	296.8776	296.8753
$[Al(SO_4)_2(H_2SO_4)]^-$	316.8567	316.8529
$[H_3Al(OH)(SO_4)_3]^-$	334.8656	334.8635
$[Al_4O_2(SO_4)_5(H_2SO_4)]^{2-}$	358.824	358.8216
$[Al_2(OH)(SO_4)_3(H_2O)]^-$	376.8354	376.8321
$[Al_4O(SO_4)_6(H_2SO_4)]^{2-}$	398.8117	398.8
$[Al(SO_4)_2(H_2SO_4)_2]^-$	414.8241	414.8203
$[Al_5O(OH)(SO_4)_7]^{2-}$	419.789	419.7843
$[HAl_2(SO_4)_4(H_2O)]^-$	456.7929	456.7889
$[Al_5O(OH)(SO_4)_7(H_2SO_4)]^{2-}$	468.7721	468.768
$[Al_6O(OH)_2(SO_4)_8]^{2-}$	489.7567	489.7523
$[Al_6O(OH)_2(SO_4)_8(H_2O)]^{2-}$	498.7605	498.7576
$[Al_5(OH)(SO_4)_8(H_2SO_4)]^{2-}$	508.7532	508.7464
$[Al_6(OH)_2(SO_4)_9]^{2-}$	529.7346	529.7307
$[Al_6(OH)_2(SO_4)_9(H_2O)]^{2-}$	538.7425	538.736
$[Al_7O_2(OH)(SO_4)_9]^{2-}$	550.7196	550.715
$[Al_7O(OH)_3(SO_4)_9]^{2-}$	559.7241	559.7203
$[Al_7O(OH)_3(SO_4)_9(H_2O)]^{2-}$	568.7255	568.7256
$[Al_6(SO_4)_{10}(H_2O)_2]^{2-}$	578.721	578.7144
$[Al_7O(OH)(SO_4)_{10}]^{2-}$	590.7014	590.6934
$[Al_7(OH)_3(SO_4)_{10}]^{2-}$	599.7048	599.6987
$[Al_8O_3(SO_4)_{10}]^{2-}$	611.6867	611.6777
$[Al_8O_3(SO_4)_{10}(H_2O)]^{2-}$	620.6903	620.683
$[Al_7(OH)(SO_4)_{11}(H_2O)]^{2-}$	639.6837	639.6771
$[Al_8O(OH)_2(SO_4)_{11}]^{2-}$	660.6694	660.6614
$[Al_8O(OH)_2(SO_4)_{11}(H_2O)]^{2-}$	669.6729	669.6667
$[Al_8(OH)_2(SO_4)_{12}]^{2-}$	700.6468	700.6398

Table S3. List of the assignments on the region of interest of the ESI-MS spectra of the solution with $[Al_{tot}] = 1$ M.

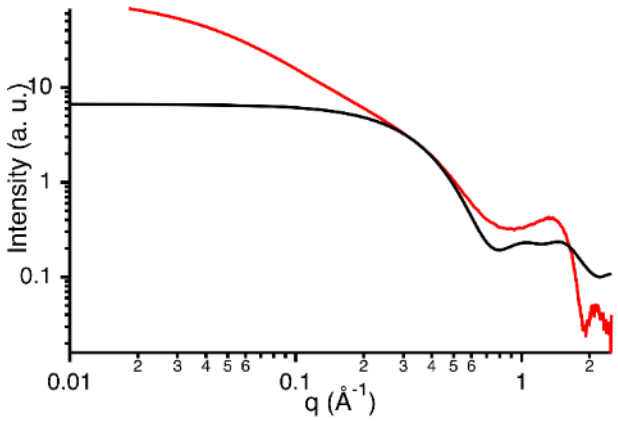

Figure S5. SWAXS curve for the as-prepared 3 M Al solution with SeO_4^{2-} counter ions (red) and a simulated curve for an $\mathbf{Al_8}$ cluster with SeO_4^{2-} counterions. These data were normalized to the Guinier region for ease of comparison.

SWAXS data indicate the solution made with H_2SeO_4(aq) contains clusters (q = 2–6 $Å^{-1}$), along with aggregated species (q = 0–2 $Å^{-1}$. The Guinier region overlaps the simulated curve (black line, Figure S4) for $\mathbf{Al_8}$ cluster scattering. The signal is too weak, however, to definitively assign the scattering to the $\mathbf{Al_8}$ cluster.

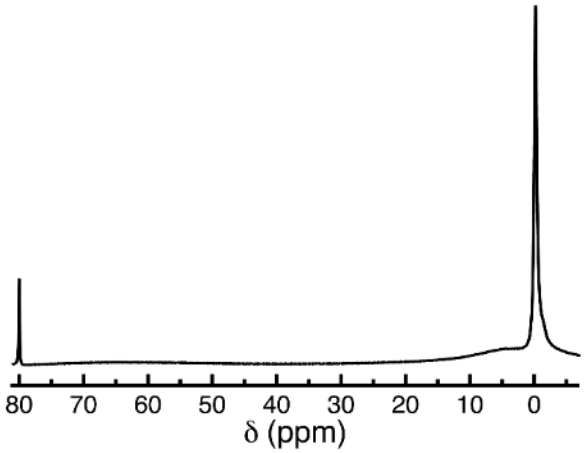

Figure S6. ^{27}Al NMR spectrum of 3-M Al^{3+} solution with SeO_4^{2-} counterions.

Similar to the 1-M Al^{3+} solution with SO_4^{2-} counterions, the ^{27}Al NMR spectrum of the SeO_4^{2-} analogue shows a peak at -1.1 ppm. This peak likely stems from the inner-sphere

selenato complex $Al(H_2O)_5(SeO_4)^+$, though the peak has not been previously reported. The peak at -1.1 ppm appears as only a shoulder in the 3-M solution (*cf.*, Figure S5).

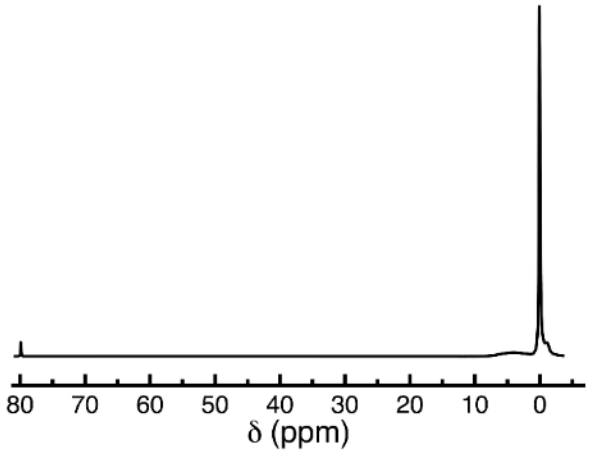

Figure S7. ^{27}Al NMR spectrum of a 1 M Al^{3+} solution with SeO_4^{2-} counterions.

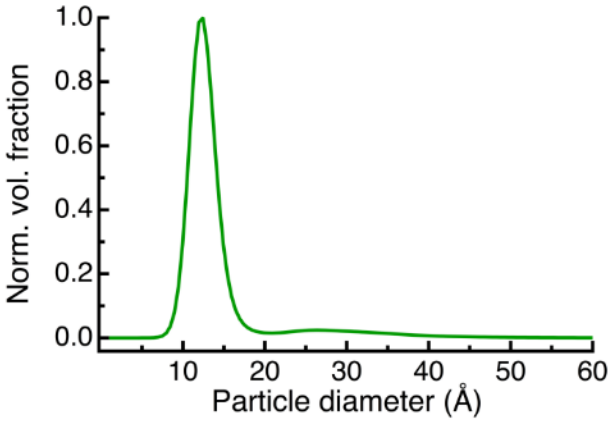

Figure S8. Particle size distribution for 3-M solution with SeO_4^{2-} counter ions.

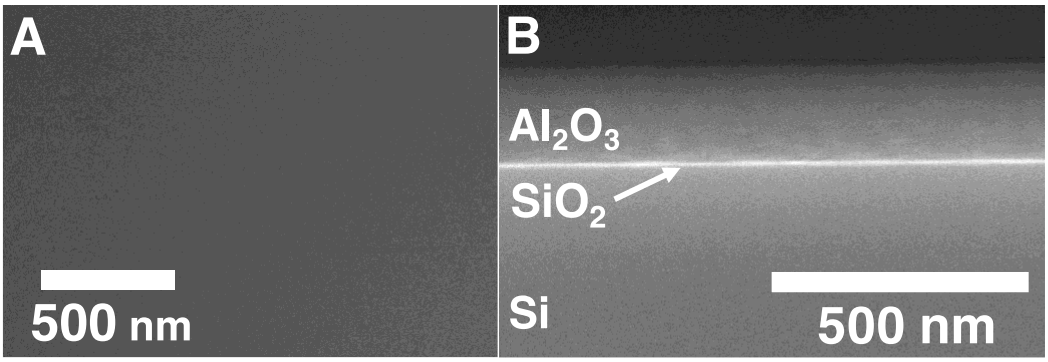

Figure S9: Top-down SEM image of a spun-coat film from the Al_8 precursor (a) and the cross-sectional view (b).

CHAPTER IV SUPPLEMENTAL INFORMATION

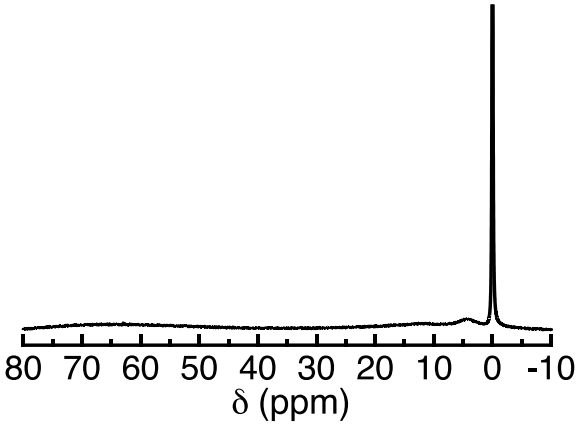

Figure S10. ^{27}Al NMR spectrum of a 1.0 M solution of the ***flat*-Al$_{13}$** prepared via dissolution with HCl.

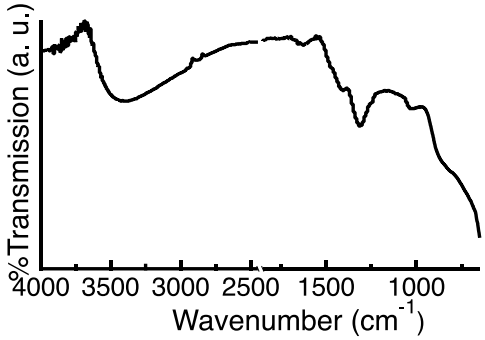

Figure S11. ATR-FTIR spectrum of the Al_2O_3 film after a 230 ºC bake for 1 min, showing stretches consistent with H_2O (3400 cm^{-1}) and hydrated NO_3 (1306 cm^{-1}).

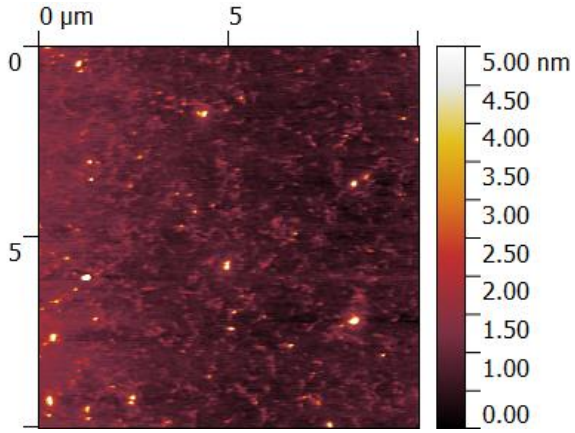

Figure S12. AFM of a film from the *flat*-Al_{13} solution annealed at 500 ºC.

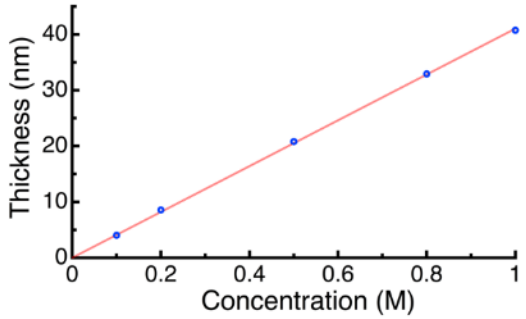

Figure S13. Thickness as a function of [Al_{tot}] for films annealed at 500 ºC (R^2 = 0.999).

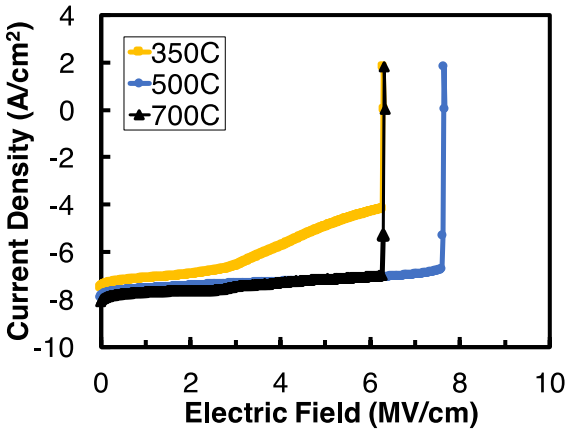

Figure S14. Representative breakdown curves for each temperature. Breakdown fields are reported using averaged measured for several devices.

CHAPTER V SUPPLEMENTAL INFORMATION

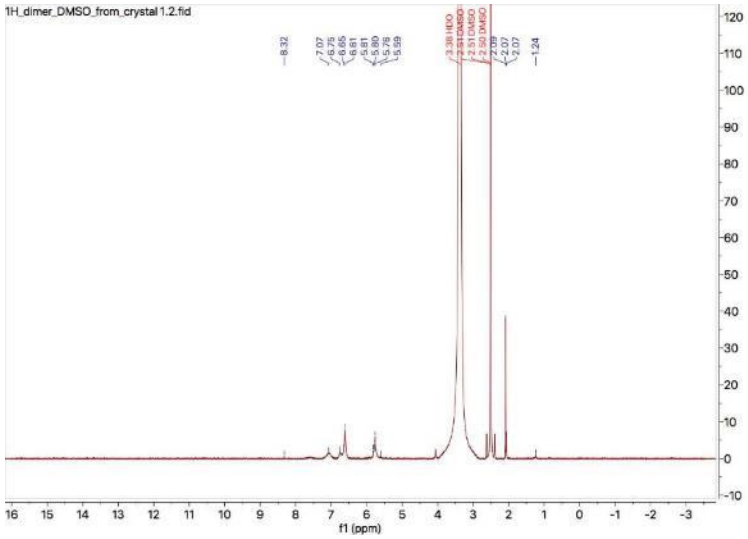

Figure S15. ^{1}H NMR of Sc_2 crystals in DMSO from a dissolution approach pathway.

REFERENCES CITED

Chapter I References

(1) Hind, A. R.; Bhargava, S. K.; Grocott, S. C. The surface chemistry of Bayer process solids: A review. *Colloids and Surfaces A: Physicochemical and Engineering Aspects*. Elsevier January 15, 1999, pp 359–374.

(2) Nazari, A.; Sanjayan, J. G. *Handbook of low carbon concrete*; Butterworth-Heinemann, 2016.

(3) Ratner, B. D. (Buddy D. . *Biomaterials science : an introduction to materials in medicine*; Academic Press, 2013.

(4) Donoghue, A. M.; Frisch, N.; Olney, D. Bauxite Mining and Alumina Refining. *J. Occup. Environ. Med.* **2014**, *56*, S12–S17 DOI: 10.1097/JOM.0000000000000001.

(5) Cui, J.; Kast, M. G.; Hammann, B. A.; Afriyie, Y.; Woods, K. N.; Plassmeyer, P. N.; Perkins, C. K.; Ma, Z. L.; Keszler, D. A.; Page, C. J.; et al. Aluminum Oxide Thin Films from Aqueous Solutions: Insights from Solid-State NMR and Dielectric Response. *Chem. Mater.* **2018**, *30* (21), 7456–7463 DOI: 10.1021/acs.chemmater.7b05078.

(6) Plassmeyer, P. N.; Archila, K.; Wager, J. F.; Page, C. J. Lanthanum Aluminum Oxide Thin-Film Dielectrics from Aqueous Solution. *ACS Appl. Mater. Interfaces* **2015**, *7* (3), 1678–1684 DOI: 10.1021/am507271e.

(7) Zhu, L.; Gao, Y.; Li, X.; Sun, X. W.; Zhang, J. Development of high-k hafnium–aluminum oxide dielectric films using sol–gel process. *J. Mater. Res.* **2014**, *29* (15), 1620–1625 DOI: 10.1557/jmr.2014.186.

(8) Woods, K. N.; Waddington, E. C.; Crump, C. A.; Bryan, E. A.; Gleckler, T. S.; Nellist, M. R.; Duell, B. A.; Nguyen, D. P.; Boettcher, S. W.; Page, C. J. Tunable high-κ $Zr_x Al_{1-x} O_y$ thin film dielectrics from all-inorganic aqueous precursor solutions. *RSC Adv.* **2017**, *7* (62), 39147–39152 DOI: 10.1039/C7RA08362A.

(9) Hayashi, Y. Hetero and lacunary polyoxovanadate chemistry: Synthesis, reactivity and structural aspects. *Coord. Chem. Rev.* **2011**, *255* (19–20), 2270–2280 DOI: 10.1016/J.CCR.2011.02.013.

(10) Hiskia, A.; Troupis, A.; Antonaraki, S.; Gkika, E.; Papaconstantinou, P. K. Polyoxometallate photocatalysis for decontaminating the aquatic environment from organic and inorganic pollutants. *Int. J. Environ. Anal. Chem.* **2006**, *86* (3–4), 233–242 DOI: 10.1080/03067310500247520.

(11) Banfield, J. F.; Welch, S. A.; Zhang, H.; Ebert, T. T.; Penn, R. L. Aggregation-based crystal growth and microstructure development in natural iron oxyhydroxide biomineralization products. *Science* **2000**, *289* (5480), 751–754 DOI: 10.1126/science.289.5480.751.

(12) Guo, H.-X.; Liu, S.-X. A novel 3D organic–inorganic hybrid based on sandwich-type cadmium hetereopolymolybdate: {[Cd4(H2O)2(2,2′-bpy)2] Cd[Mo6O12(OH)3(PO4)2(HPO4)2]2}[Mo2O4(2,2′-bpy)2]2 · 3H2O. *Inorg. Chem. Commun.* **2004**, *7* (11), 1217–1220 DOI: 10.1016/J.INOCHE.2004.09.010.

(13) Sun, X.; Sun, Y.; Yu, J. Crystal structure of aluminum sulfate hexadecahydrate and its morphology. *Cryst. Res. Technol.* **2015**, *50* (4), 293–298 DOI: 10.1002/crat.201400428.

(14) Johansson, G.; Lundgren, G.; Sillén, L. G.; Söderquist, R. On the Crystal Structure of a Basic Aluminium Sulfate and the Corresponding Selenate. *Acta Chem. Scand.* **2008** DOI: 10.3891/acta.chem.scand.14-0769.

(15) Lee, A. P.; Phillips, B. L.; Olmstead, M. M.; Casey, W. H. Synthesis and Characterization of the GeO 4 Al 12 (OH) 24 (OH 2) 12 8+ Polyoxocation. *Inorg. Chem.* **2001**, *40* (17), 4485–4487 DOI: 10.1021/ic010146e.

(16) Parker, W. O.; Millini, R.; Kiricsi, I. Metal Substitution in Keggin-Type Tridecameric Aluminum−Oxo−Hydroxy Clusters. *Inorg. Chem.* **1997**, *36* (4), 571–575 DOI: 10.1021/ic960635s.

(17) Casey, W. H. Large aqueous aluminum hydroxide molecules. *Chem. Rev.* **2006**, *106* (1), 1–16 DOI: 10.1021/cr040095d.

(18) Sulpizi, M.; Lützenkirchen, J. Atypical titration curves for $GaAl_{12}$ Keggin-ions explained by a joint experimental and simulation approach. *J. Chem. Phys.* **2018**, *148* (22), 222836 DOI: 10.1063/1.5024201.

(19) Michot, L. J.; Montargès-Pelletier, E.; Lartiges, B. S.; d'Espinose de la Caillerie, J.-B.; Briois, V. Formation Mechanism of the Ga 13 Keggin Ion: A Combined EXAFS and NMR Study. *J. Am. Chem. Soc.* **2000**, *122* (25), 6048–6056 DOI: 10.1021/ja9941429.

(20) Bradley, S. M.; Kydd, R. A.; Yamdagni, R.; Fyfe, C. A. Ga13, GaAl12, and Al13 Polyoxocations and Pillared Clays. In *Expanded Clays and Other Microporous Solids*; Springer US: Boston, MA, 1992; pp 13–31.

(21) Seichter, W.; Mögel, H.-J.; Brand, P.; Salah, D. Crystal Structure and Formation of the Aluminium Hydroxide Chloride [Al13(OH)24(H2O)24]Cl15 · 13 H2O. *Eur. J. Inorg. Chem.* **1998**, *1998* (6), 795–797 DOI: 10.1002/(SICI)1099-0682(199806)1998:6<795::AID-EJIC795>3.0.CO;2-A.

(22) Rather, E.; Gatlin, J. T.; Nixon, P. G.; Tsukamoto, T.; Kravtsov, V.; Johnson, D. W. A simple organic reaction mediates the crystallization of the inorganic nanocluster [Ga13(μ3-OH)6(μ2- OH)18(H2O)24](NO3)15. *J. Am. Chem. Soc.* **2005**, *127* (10), 3242–3243.

(23) Gatlin, J. T.; Mensinger, Z. L.; Zakharov, L. N.; MacInnes, D.; Johnson, D. W. Facile synthesis of the tridecameric Al13 nanocluster Al 13(??3-OH)6(??2-OH) 18(H2O)24(NO3)15. *Inorg. Chem.* **2008**, *47* (4), 1267–1269.

(24) Wang, W.; Wentz, K. M.; Hayes, S. E.; Johnson, D. W.; Keszler, D. A. Synthesis of the hydroxide cluster [Al13(μ3-OH)6(μ-OH)18(H2O)24]15+ from an aqueous solution. *Inorg. Chem.* **2011**, *50*, 4683–4685 DOI: 10.1021/ic200483q.

(25) Wang, W.; Liu, W.; Chang, I.-Y.; Wills, L. a; Zakharov, L. N.; Boettcher, S. W.; Cheong, P. H.-Y.; Fang, C.; Keszler, D. a. Electrolytic synthesis of aqueous aluminum nanoclusters and in situ characterization by femtosecond Raman spectroscopy and computations. *Proc. Natl. Acad. Sci. U. S. A.* **2013**, *110*, 18397–18401 DOI: 10.1073/pnas.1315396110.

(26) Kamunde-Devonish, M. K.; Jackson, M. N.; Mensinger, Z. L.; Zakharov, L. N.; Johnson, D. W. Transmetalation of aqueous inorganic clusters: A useful route to the synthesis of heterometallic aluminum and indium hydroxo-aquo clusters. *Inorg. Chem.* **2014**, *53*, 7101–7105 DOI: 10.1021/ic403121r.

(27) Abeysinghe, S.; Unruh, D. K.; Forbes, T. Z. Surface modification of Al30 Keggin-type polyaluminum molecular clusters. *Inorg. Chem.* **2013**, *52* (10), 5991–5999 DOI: 10.1021/ic400321k.

(28) Abeysinghe, S.; Unruh, D. K.; Forbes, T. Z. Crystallization of Keggin-Type Polyaluminum Species by Supramolecular Interactions with Disulfonate Anions. *Cryst. Growth Des.* **2012**, *12* (4), 2044–2051 DOI: 10.1021/cg3000087.

(29) Casey, W. H.; Olmstead, M. M.; Phillips, B. L. A new aluminum hydroxide octamer, [Al8(OH)14(H2O)18](SO4)5 x 16H2O. *Inorg. Chem.* **2005**, *44* (14), 4888–4890 DOI: 10.1021/ic050426k.

Chapter II References

(1) W. Seichter, H.-J. Mögel, P. Brand, D. Salah, *Eur. J. Inorg. Chem.* **1998**, *1998*, 795–797.

(2) W. Wang, K. M. Wentz, S. E. Hayes, D. W. Johnson, D. A. Keszler, *Inorg. Chem.* **2011**, *50*, 4683–4685.

(3) S. E. Smart, J. Vaughn, I. Pappas, L. Pan, *Chem. Commun.* **2013**, *49*, 11352–11354.

(4) G. Johansson, G. Lundgren, L. Gunnar Sillén, R. Söderquist, *Acta Chem. Scand.* **1960**, *14*, 769–771.

(5) L. Allouche, C. Gérardin, T. Loiseau, G. Férey, F. Taulelle, *Angew. Chemie* **2000**, *112*, 521–524.

(6) S. Abeysinghe, D. K. Unruh, T. Z. Forbes, *Cryst. Growth Des.* **2012**, *12*, 2044–2051.

(7) W. H. Casey, M. M. Olmstead, B. L. Phillips, *Inorg. Chem.* **2005**, *44*, 4888–4890.

(8) K. S. Lokare, N. Frank, B. Braun-Cula, I. Goikoetxea, J. Sauer, C. Limberg, *Angew. Chemie Int. Ed.* **2016**, *55*, 12325–12329; *Angew. Chem.* **2016**, *128*, 12513–12517.

(9) G. Sposito, *The Environmental Chemistry of Aluminum*, CRC Press LLC, Boca Raton, FL, **1996**.

(10) T. A. Stewart, D. E. Trudell, T. M. Alam, C. A. Ohlin, C. Lawler, W. H. Casey, S. Jett, M. Nyman, *Environ. Sci. Technol.* **2009**, *43*, 5416–5422.

(11) C. R. Armstrong, W. H. Casey, A. Navrotsky, *Proc. Natl. Acad. Sci.* **2011**, *108*, 14775–14779.

(12) D. A. Keszler, J. T. Anderson, S. T. Meyers, in *Solut. Process. Mater.* (Ed.: D.B. Mitzi), **2009**, pp. 109–127.

(13) R. P. Oleksak, R. E. Ruther, F. Luo, K. C. Fairley, S. R. Decker, W. F. Stickle, D. W. Johnson, E. L. Garfunkel, G. S. Herman, D. A. Keszler, *ACS Appl. Mater. Interfaces* **2014**, *6*, 2917–2921.

(14) J. W. Akitt, N. N. Greenwood, B. L. Khandelwal, *J. Chem. Soc. Dalt. Trans.* **1972**, 1226–1229.

(15) J. W. Akitt, J. M. Elders, *J. Chem. Soc. Farad. T.* **1985**, *81*, 1923–1930.

(16) J. W. Akitt, J. M. Elders, *J. Chem. Soc. Dalt. Trans.* **1988**, 1347–1355.

(17) M. N. Jackson, M. K. Kamunde-Devonish, B. A. Hammann, L. A. Wills, L. B. Fullmer, S. E. Hayes, P. H.-Y. Cheong, W. H. Casey, M. Nyman, D. W. Johnson, *Dalton Trans.* **2015**, *44*, 16982–17006.

(18) S. Goberna-Ferrón, D.-H. Park, J. M. Amador, D. A. Keszler, M. Nyman, *Angew. Chemie Int. Ed.* **2016**, *55*, 6221–6224; *Angew. Chem.* **2016**, *128*, 6329–6333.

(19) L. B. Fullmer, R. H. Mansergh, L. N. Zakharov, D. A. Keszler, M. Nyman, *Cryst. Growth Des.* **2015**, *15*, 3885–3892.

(20) A. F. Oliveri, E. W. Elliott, M. E. Carnes, J. E. Hutchison, D. W. Johnson, *ChemPhysChem* **2013**, *14*, 2655–61.

(21) G. Johansson, *Acta Chem. Scand.* **1962**, *16*, 403–420.

(22) S. W. Smith, W. Wang, D. A. Keszler, J. F. Conley, *J. Vac. Sci. Technol. A Vacuum, Surfaces, Film.* **2014**, *32*, 41501.

(23) C. K. Perkins, R. H. Mansergh, J. C. Ramos, C. E. Nanayakkara, D.-H. Park, S. Goberna-Ferrón, L. B. Fullmer, J. T. Arens, M. T. Gutierrez-Higgins, Y. R. Jones, J. I. Lopez, T. M. Rowe, D. M. Whitehurst, M. Nyman, Y. J. Chabal, D. A. Keszler, *Opt. Mater. Express* **2017**, *7*, 273–280.

(24) S. T. Meyers, J. T. Anderson, D. Hong, C. M. Hung, J. F. Wager, D. A. Keszler, *Chem. Mater.* **2007**, *19*, 4023–4029.

(25) K. Jiang, J. T. Anderson, K. Hoshino, D. Li, J. F. Wager, D. A. Keszler, *Chem. Mater.* **2011**, *23*, 945–952.

(26) J. T. Anderson, C. L. Munsee, C. M. Hung, T. M. Phung, G. S. Herman, D. C. Johnson, J. F. Wager, D. A. Keszler, *Adv. Funct. Mater.* **2007**, *17*, 2117–2124.

Chapter III References

(1) S. Abeysinghe, D. K. Unruh, T. Z. Forbes, Cryst. Growth Des. 2012, 12, 2044–2051.

(2) Z. Sun, H. Wang, Y. Zhang, J. Li, Y. Zhao, W. Jiang, L. Wang, Dalton Trans. 2013, 42, 12956–64.

(3) Z. Sun, H. Wang, H. Tong, S. Sun, Inorg. Chem. 2011, 50, 559–64.

(4) G. Fu, L. F. Nazar, A. D. Bain, Chem. Mater. 1991, 3, 602–610.

(5) J. Rowsell, L. F. Nazar, J. Am. Chem. Soc. 2000, 122, 3777–3778.

(6) L. Allouche, C. Gérardin, T. Loiseau, G. Férey, F. Taulelle, Angew. Chemie 2000, 112, 521–524.

(7) W. Seichter, H.-J. Mögel, P. Brand, D. Salah, Eur. J. Inorg. Chem. 1998, 1998, 795–797.

(8) W. Wang, K. M. Wentz, S. E. Hayes, D. W. Johnson, D. A. Keszler, Inorg. Chem. 2011, 50, 4683–4685.

(9) W. Schmitt, E. Baissa, A. Mandel, C. E. Anson, A. K. Powell, Angew. Chemie Int. Ed. 2001, 40, 3577–3581.

(10) W. H. Casey, M. M. Olmstead, B. L. Phillips, Inorg. Chem. 2005, 44, 4888–4890.

(11) W. H. Casey, Chem. Rev. 2006, 106, 1–16.

(12) B. L. Phillips, C. A. Ohlin, J. Vaughn, W. Woerner, S. Smart, R. Subramanyam, L. Pan, Inorg. Chem. 2016, 55, 12270–12280.

(13) C. D. Pilgrim, J. R. Callahan, C. A. Colla, C. A. Ohlin, H. E. Mason, W. H. Casey, Dalt. Trans. 2017, 46, 2249–2254.

(14) L. Allouche, C. Huguenard, F. Taulelle, J. Phys. Chem. Solids 2001, 62, 1525–1531.

(15) A. F. Oliveri, C. A. Colla, C. K. Perkins, N. Akhavantabib, J. R. Callahan, C. D. Pilgrim, S. E. Smart, P. H.-Y. Cheong, L. Pan, W. H. Casey, Chem. – A Eur. J. 2016, 22, 18682–18685.

(16) C. K. Perkins, E. S. Eitrheim, B. L. Fulton, L. B. Fullmer, C. A. Colla, D. H. Park, A. F. Oliveri, J. E. Hutchison, M. Nyman, W. H. Casey, et al., Angew. Chemie - Int. Ed. 2017, 56, 10161–10164.

(17) B. L. Fulton, C. K. Perkins, R. H. Mansergh, M. A. Jenkins, V. Gouliouk, M. N. Jackson, J. C. Ramos, N. M. Rogovoy, M. T. Gutierrez-Higgins, S. W. Boettcher, et al., Chem. Mater. 2017, 29, 7760–7765.

(18) G. Johansson, G. Lundgren, L. Gunnar Sillén, R. Söderquist, Acta Chem. Scand. 1960, 14, 769–771.

(19) A. . Kunwar, A. . Thompson, H. . Gutowsky, E. Oldfield, J. Magn. Reson. 1984, 60, 467–472.

(20) L. Allouche, F. Taulelle, Inorg. Chem. Commun. 2003, 6, 1167–1170.

(21) S. E. Smart, J. Vaughn, I. Pappas, L. Pan, Chem. Commun. 2013, 49, 11352–11354.

(22) G. Furrer, C. Ludwig, P. W. Schindler, J. Colloid Interface Sci. 1992, 149, 56–67.

(23) J. H. Son, Y.-U. Kwon, O. Hee Han, Inorg. Chem. 2003, 42, 4153–4159.

(24) S. Abeysinghe, D. K. Unruh, T. Z. Forbes, Inorg. Chem. 2013, 52, 5991–5999.

(25) K. Mizuno, T. Mura, S. Uchida, Cryst. Growth Des. 2016, 16, 4968–4974.

(26) B. Gu, C. Sun, J. C. Fettinger, W. H. Casey, A. Dikhtiarenko, J. Gascon, K. Koichumanova, K. Babu, E. Heeres, S. He, Chem. Commun. 2018.

(27) C. A. Ohlin, J. R. Rustad, W. H. Casey, Dalt. Trans. 2014, 43, 14533–14536.

Chapter IV References

(1) Sposito, G. *The Environmental Chemistry of Aluminum*; 2nd ed.; CRC Press LLC: Boca Raton, FL, 1996.

(2) Basim, G. B.; Adler, J. J.; Mahajan, U.; Singh, R. K.; Moudgil, B. M. Effect of Particle Size of Chemical Mechanical Polishing Slurries for Enhanced Polishing with Minimal Defects. *J. Electrochem. Soc.* **2000**, *147*, 3523–3528.

(3) Bell, A. T. The Impact of Nanoscience on Heterogeneous Catalysis. *Science* **2003**, *299*, 1688–1691.

(4) Abeysinghe, S.; Unruh, D. K.; Forbes, T. Z. Crystallization of Keggin-Type Polyaluminum Species by Supramolecular Interactions with Disulfonate Anions. *Cryst. Growth Des.* **2012**, *12*, 2044–2051.

(5) Fu, G.; Nazar, L. F.; Bain, A. D. Aging Processes of Alumina Sol-Gels: Characterization of New Aluminum Polyoxycations by ^{27}Al NMR Spectroscopy. *Chem. Mater.* **1991**, *3*, 602–610.

(6) Johansson, G.; Lundgren, G.; Gunnar Sillén, L.; Söderquist, R. On the Crystal Structure of a Basic Aluminum Sulfate and the Correspnding Selenate. *Acta Chem. Scand.* **1960**, *14*, 769–771.

(7) Smart, S. E.; Vaughn, J.; Pappas, I.; Pan, L. Controlled Step-Wise Isomerization of the Keggin-Type Al_{13} and Determination of the γ-Al_{13} Structure. *Chem. Commun.* **2013**, *49*, 11352–11354.

(8) Seichter, W.; Mögel, H.-J.; Brand, P.; Salah, D. Crystal Structure and Formation of the Aluminium Hydroxide Chloride $[Al_{13}(OH)_{24}(H_2O)_{24}]Cl_{15} \cdot 13\ H_2O$. *Eur. J. Inorg. Chem.* **1998**, *1998*, 795–797.

(9) Wang, W.; Wentz, K. M.; Hayes, S. E.; Johnson, D. W.; Keszler, D. A. Synthesis of the Hydroxide Cluster $[Al_{13}(\mu_3\text{-}OH)_6(\mu\text{-}OH)_{18}(H_2O)_{24}]^{15+}$ from an Aqueous Solution. *Inorg. Chem.* **2011**, *50*, 4683–4685.

(10) Gatlin, J. T.; Mensinger, Z. L.; Zakharov, L. N.; MacInnes, D.; Johnson, D. W. Facile Synthesis of the Tridecameric Al_{13} Nanocluster $Al_{13}(\mu_3\text{-}OH)_6(\mu\text{-}OH)_{18}(H_2O)_{24}(NO_3)_{15}$. *Inorg. Chem.* **2008**, *47*, 1267–1269.

(11) Perkins, C. K.; Eitrheim, E. S.; Fulton, B. L.; Fullmer, L. B.; Colla, C. A.; Park, D.-H.; Oliveri, A. F.; Hutchison, J. E.; Nyman, M.; Casey, W. H.; Johnson, D. W.; Keszler, D. A. Synthesis of an Aluminum Hydroxide Octamer through a Simple Dissolution Method. *Angew. Chemie Int. Ed.* **2017**, *56*, 10161–10164; *Angew. Chemie* **2017**, *129*, 10295–10298.

(12) Perkins, C. K.; Mansergh, R. H.; Ramos, J. C.; Nanayakkara, C. E.; Park, D.-H.; Goberna-Ferrón, S.; Fullmer, L. B.; Arens, J. T.; Gutierrez-Higgins, M. T.; Jones, Y. R.; Lopez, J. I.; Rowe, T. M.; Whitehurst, D. M; Chabal, Y. J.; Keszler, D. A. Low-Index, Smooth Al_2O_3 Films by Aqueous Solution Process. *Opt. Mater. Express* **2017**, *7*, 273–280.

(13) Smith, S. W.; Wang, W.; Keszler, D. A.; Conley, J. F. Solution Based Prompt Inorganic Condensation and Atomic Layer Deposition of Al_2O_3 Films: A Side-by-Side Comparison. *J. Vac. Sci. Technol. A Vacuum, Surfaces, Film.* **2014**, *32*, 41501.

(14) Kamunde-Devonish, M. K.; Jackson, M. N.; Mensinger, Z. L.; Zakharov, L. N.; Johnson, D. W. Transmetalation of Aqueous Inorganic Clusters: A Useful Route to the Synthesis of Heterometallic Aluminum and Indium Hydroxo-Aquo Clusters. *Inorg. Chem.* **2014**, *53*, 7101–7105.

(15) Nadarajah, A.; Wu, M. Z. B.; Archila, K.; Kasti, M. G.; Smith, A. M.; Chiang, T. H.; Keszler, D. A.; Wager, J. F.; Boettcher, S. W. Amorphous In-Ga-Zn Oxide Semiconducting Thin Films with High Mobility from Electrochemically Generated Aqueous Nanocluster Inks. *Chem. Mater.* **2015**, *27*, 5587–5596.

(16) Carnes, M. E.; Knutson, C. C.; Nadarajah, A.; Jackson, M. N.; Oliveri, A. F.; Norelli, K. M.; Crockett, B. M.; Bauers, S. R.; Moreno-Luna, H. A.; Taber, B. N.; Pacheco, D. J.; Olson, J. Z.; Brevick, K. R.; Sheehan, C. E.; Johnson, D. W.; Boettcher, S. W. Electrochemical Synthesis of Flat-$[Ga_{13-x}In_x(\mu_3\text{-}OH)_6(\mu\text{-}OH)_{18}(H_2O)_{24}(NO_3)_{15}]$ Clusters as Aqueous Precursors for Solution-Processed Semiconductors. *J. Mater. Chem. C* **2014**, *2*, 8492–8496.

(17) Mensinger, Z. L.; Gatlin, J. T.; Meyers, S. T.; Zakharov, L. N.; Keszler, D. A.; Johnson, D. W. Synthesis of Heterometallic Group 13 Nanoclusters and Inks for Oxide Thin-Film Transistors. *Angew. Chemie Int. Ed.* **2008**, *47*, 9484–9486.

(18) Marsh, D. A.; Goberna-Ferron, S.; Baumeister, M. K.; Zakharov, L. N.; Nyman, M.; Johnson, D. W. Ln Polyoxocations: Yttrium Oxide Solution Speciation & Solution Deposited Thin Films. *Dalt. Trans.* **2017**, *46*, 947–955.

(19) Wood, S. R.; Woods, K. N.; Plassmeyer, P. N.; Marsh, D. A.; Johnson, D. W.; Page, C. J.; Jensen, K. M. Ø.; Johnson, D. C. Same Precursor, Two Different Products: Comparing the Structural Evolution of In–Ga–O "Gel-Derived" Powders and Solution-Cast Films Using Pair Distribution Function Analysis. *J. Am. Chem. Soc.* **2017**, *139*, 5607–5613.

(20) Plassmeyer, P. N.; Archila, K.; Wager, J. F.; Page, C. J. Lanthanum Aluminum Oxide Thin-Film Dielectrics from Aqueous Solution. *ACS Appl. Mater. Interfaces* **2015**, *7*, 1678–1684.

(21) Nadarajah, A.; Carnes, M. E.; Kast, M. G.; Johnson, D. W.; Boettcher, S. W. Aqueous Solution Processing of F-Doped SnO_2 Transparent Conducting Oxide Films Using a Reactive Tin(II) Hydroxide Nitrate Nanoscale Cluster. *Chem. Mater.* **2013**, *25*, 4080–4087.

(22) Wang, W.; Liu, W.; Chang, I.-Y.; Wills, L. A.; Zakharov, L. N.; Boettcher, S. W.; Cheong, P. H.-Y.; Fang, C.; Keszler, D. A. Electrolytic Synthesis of Aqueous Aluminum Nanoclusters and in Situ Characterization by Femtosecond Raman Spectroscopy and Computations. *Proc. Natl. Acad. Sci.* **2013**, *110*, 18397–18401.

(23) Jackson, M. N.; Wills, L. A.; Chang, I. Y.; Carnes, M. E.; Scatena, L. F.; Cheong, P. H. Y.; Johnson, D. W. Identifying Nanoscale M13 Clusters in the Solid State and Aqueous Solution: Vibrational Spectroscopy and Theoretical Studies. *Inorg. Chem.* **2013**, *52*, 6187–6192.

(24) Kumar, P.; Wiedmann, M. K.; Winter, C. H.; Avrutsky, I. Optical Properties of Al_2O_3 Thin Films Grown by Atomic Layer Deposition. *Appl. Opt.* **2009**, *48*, 5407–5412.

(25) Tadanaga, K.; Kitamuro, K.; Matsuda, A.; Minami, T. Formation of Superhydrophobic Alumina Coating Films with High Transparency on Polymer Substrates by the Sol-Gel Method. *J. Sol-Gel Sci. Technol.* **2003**, *26*, 705–708.

(26) Tadanaga, K.; Katata, N.; Minami, T. Super-Water-Repellent Al_2O_3 Coating Films with High Transparency. *J. Am. Ceram. Soc.* **1997**, *80*, 1040–1042.

(27) Schütze, A.; Quinto, D. T. Pulsed Plasma-Assisted PVD Sputter-Deposited Alumina Thin Films. *Surf. Coatings Technol.* **2003**, *162*, 174–182.

(28) Segda, B. G.; Jacquet, M.; Besse, J. P. Elaboration, Characterization and Dielectric Properties Study of Amorphous Alumina Thin Films Deposited by R.f. Magnetron Sputtering. *Vacuum* **2001**, *62*, 27–38.

(29) Xu, W.; Wang, H.; Xie, F.; Chen, J.; Cao, H.; Xu, J.-B. Facile and Environmentally Friendly Solution-Processed Aluminum Oxide Dielectric for Low-Temperature, High-Performance Oxide Thin-Film Transistors. *ACS Appl. Mater. Interfaces* **2015**, *7*, 5803–5810.

(30) Liu, A.; Liu, G.; Zhu, H.; Shin, B.; Fortunato, E.; Martins, R.; Shan, F. Eco-Friendly Water-Induced Aluminum Oxide Dielectrics and Their Application in a Hybrid Metal Oxide/polymer TFT. *RSC Adv.* **2015**, *5*, 86606–86613.

(31) Branquinho, R.; Salgueiro, D.; Santos, L.; Barquinha, P.; Pereira, L.; Martins, R.; Fortunato, E. Aqueous Combustion Synthesis of Aluminum Oxide Thin Films and Application as Gate Dielectric in GZTO Solution-Based TFTs. *ACS Appl. Mater. Interfaces* **2014**, *6*, 19592–19599.

(32) Hale, J.; Johs, B. CompleteEASE. *CompleteEASE* **2012**.

Chapter V References

(1) Moore, G. E. Cramming more components onto integrated circuits, Reprinted from Electronics, volume 38, number 8, April 19, 1965, pp.114 ff. *IEEE Solid-State Circuits Soc. Newsl.* **2006**, *11* (3), 33–35 DOI: 10.1109/N-SSC.2006.4785860.

(2) Acosta, G. *SCANDIUM OXIDE THIN FILMS AND THEIR OPTICAL PROPERTIES IN THE EXTREME ULTRAVIOLET*; 2007.

(3) Dixon, S. C.; Jiamprasertboon, A.; Carmalt, C. J.; Parkin, I. P. Luminescence behaviour and deposition of Sc2O3thin films from scandium(III) acetylacetonate at ambient pressure. *Appl. Phys. Lett.* **2018**, *112* (22), 221902 DOI: 10.1063/1.5038636.

(4) Krous, E. CHARACTERIZATION OF SCANDIUM OXIDE THIN FILMS FOR USE IN INTERFERENCE COATINGS FOR HIGH-POWER LASERS OPERATING IN THE NEAR-INFRARED. **2010**.

(5) Akiyama, M.; Kamohara, T.; Kano, K.; Teshigahara, A.; Takeuchi, Y.; Kawahara, N. Enhancement of Piezoelectric Response in Scandium Aluminum Nitride Alloy Thin Films Prepared by Dual Reactive Cosputtering. *Adv. Mater.* **2009**, *21* (5), 593–596 DOI: 10.1002/adma.200802611.

(6) Akiyama, M.; Kano, K.; Teshigahara, A. Influence of growth temperature and scandium concentration on piezoelectric response of scandium aluminum nitride alloy thin films. *Appl. Phys. Lett.* **2009**, *95* (16), 162107 DOI: 10.1063/1.3251072.

(7) Fulton, B. L.; Perkins, C. K.; Mansergh, R. H.; Jenkins, M. A.; Gouliouk, V.; Jackson, M. N.; Ramos, J. C.; Rogovoy, N. M.; Gutierrez-Higgins, M. T.; Boettcher, S. W.; et al. Minerals to Materials: Bulk Synthesis of Aqueous Aluminum Clusters and Their Use as Precursors for Metal Oxide Thin Films. *Chem. Mater.* **2017**, *29* (18), 7760–7765 DOI: 10.1021/acs.chemmater.7b02106.

(8) Constable, E. C. Scandium. *Coord. Chem. Rev.* **1985**, *62*, 131–143 DOI: 10.1016/0010-8545(85)80017-5.

(9) Kilpatrick, M.; Pokras, L. Acid Dissociation of the Aquoscandium Ions. *J. Electrochem. Soc.* **1953**, *100* (2), 85 DOI: 10.1149/1.2781089.

(10) Aveston, J. Hydrolysis of scandium(III): ultracentrifugation and acidity measurements. *J. Chem. Soc. A Inorganic, Phys. Theor.* **1966**, *0* (0), 1599 DOI: 10.1039/j19660001599.

(11) Brown, P. L.; Ellis, J.; Sylva, R. N. The hydrolysis of metal ions. Part 6. Scandium(III). *J. Chem. Soc. Dalt. Trans.* **1983**, *0* (1), 35 DOI: 10.1039/dt9830000035.

(12) Haid, E.; Köhnlein, D.; Kössler, G.; Lutz, O.; Messner, W.; Mohn, K. R.; Nothaft, G.; Van Rickelen, B.; Schich, W.; Steinhauser, N. *Scandium NMR Investigations in Aqueous Solutions*; 1983; Vol. 38.

(13) Deakin, L.; Levason, W.; Popham, M. C.; Reid, G.; Webster, M. Syntheses, structures and multinuclear NMR (45Sc, 89Y, 31P) studies of Ph3PO, Ph2MePO and Me3PO complexes of scandium and yttrium nitrates. *J. Chem. Soc. Dalt. Trans.* **2000**, *0* (14), 2439–2447 DOI: 10.1039/b001669l.

(14) Brown, M. D.; Levason, W.; Murray, D. C.; Popham, M. C.; Reid, G.; Webster, M. Primary and secondary coordination of crown ethers to scandium(III). Synthesis, properties and structures of the reaction products of ScCl3(thf)3, ScCl3·6H2O and Sc(NO3)3·5H2O with crown ethers. *Dalt. Trans.* **2003**, *0* (5), 857–865 DOI: 10.1039/b210458j.

(15) Wang, W.; Chang, I.; Zakharov, L.; Cheong, P. H.; Keszler, D. A. Wei Wang, I-Ya Chang, Lev Zakharov, Paul Ha-Yeon Cheong, and Douglas A. Keszler *. **2013**, *2* (3), 1807–1811.